Research Article

TRANSPARENT PROCESS OPEN ACCESS

EMBO Molecular Medicine

The GPR120 agonist TUG-891 promotes metabolic health by stimulating mitochondrial respiration in brown fat

Maaike Schilperoort[1,2,3,*], Andrea D van Dam[2,3], Geerte Hoeke[2,3], Irina G Shabalina[4], Anthony Okolo[5], Aylin C Hanyaloglu[5], Lea H Dib[6], Isabel M Mol[2,3], Natarin Caengprasath[5], Yi-Wah Chan[7], Sami Damak[8], Anne Reifel Miller[9], Tamer Coskun[9], Bharat Shimpukade[10], Trond Ulven[10], Sander Kooijman[2,3], Patrick CN Rensen[2,3] & Mark Christian[1,**]

Abstract

Brown adipose tissue (BAT) activation stimulates energy expenditure in human adults, which makes it an attractive target to combat obesity and related disorders. Recent studies demonstrated a role for G protein-coupled receptor 120 (GPR120) in BAT thermogenesis. Here, we investigated the therapeutic potential of GPR120 agonism and addressed GPR120-mediated signaling in BAT. We found that activation of GPR120 by the selective agonist TUG-891 acutely increases fat oxidation and reduces body weight and fat mass in C57Bl/6J mice. These effects coincided with decreased brown adipocyte lipid content and increased nutrient uptake by BAT, confirming increased BAT activity. Consistent with these observations, GPR120 deficiency reduced expression of genes involved in nutrient handling in BAT. Stimulation of brown adipocytes *in vitro* with TUG-891 acutely induced O_2 consumption, through GPR120-dependent and GPR120-independent mechanisms. TUG-891 not only stimulated GPR120 signaling resulting in intracellular calcium release, mitochondrial depolarization, and mitochondrial fission, but also activated UCP1. Collectively, these data suggest that activation of brown adipocytes with the GPR120 agonist TUG-891 is a promising strategy to increase lipid combustion and reduce obesity.

Keywords brown adipose tissue; Ca^{2+}; GPR120; lipid metabolism; mitochondria

Subject Categories Metabolism; Pharmacology & Drug Discovery

DOI 10.15252/emmm.201708047 | Received 23 May 2017 | Revised 20 December 2017 | Accepted 22 December 2017

EMBO Mol Med (2018) e8047

Introduction

Brown adipose tissue (BAT) is present and active in human adults and contributes to total energy expenditure (EE) (Cypess *et al*, 2009; van Marken Lichtenbelt *et al*, 2009; Virtanen *et al*, 2009). This contrasts with white adipose tissue (WAT), which primarily serves as a site of energy storage. Cold exposure, the natural stimulus of BAT, increases the volume and activity of metabolically active BAT and reduces fat mass in adult human subjects (van der Lans *et al*, 2013; Yoneshiro *et al*, 2013; Blondin *et al*, 2014). Cold exposure stimulates the sympathetic nervous system to release norepinephrine, which in turn activates brown adipocytes through the β3-adrenergic receptor (ADRB3) (Argyropoulos & Harper, 2002). Activation of brown adipocytes initiates intracellular signaling cascades, resulting in the breakdown of triglycerides (TG) stored in intracellular lipid droplets to yield fatty acids (FA) and glycerol (Cannon & Nedergaard, 2004). The FAs are subsequently transported to the mitochondria where they are either oxidized or used to allosterically activate uncoupling protein-1 (UCP1), which is present in the inner membrane of mitochondria (Fedorenko *et al*, 2012; Nicholls, 2017). UCP1 disrupts the proton gradient that is required for ATP synthesis, resulting in the release of energy as heat instead of ATP: a process called thermogenesis (Trayhurn, 2017). Since activated BAT burns high amounts of FAs, it is considered an

1 Division of Biomedical Sciences, Warwick Medical School, University of Warwick, Coventry, UK
2 Division of Endocrinology, Department of Medicine, Leiden University Medical Center, Leiden, The Netherlands
3 Einthoven Laboratory for Experimental Vascular Medicine, Leiden, The Netherlands
4 Department of Molecular Biosciences, The Wenner-Gren Institute, The Arrhenius Laboratories F3, Stockholm University, Stockholm, Sweden
5 Department of Surgery and Cancer, Institute of Reproductive and Developmental Biology, Imperial College London, London, UK
6 Institute of Cardiovascular Sciences, College of Medical and Dental Sciences, University of Birmingham, Birmingham, UK
7 Lymphocyte Development Group, MRC London Institute of Medical Sciences, Hammersmith Campus, Imperial College London, London, UK
8 Nestlé Research Center, Lausanne, Switzerland
9 Lilly Research Laboratories, Diabetes/Endocrine Department, Lilly Corporate Center, Indianapolis, IN, USA
10 Department of Physics, Chemistry and Pharmacy, University of Southern Denmark, Odense, Denmark
*Corresponding author. Tel: +31-71-5265304. E-mail: m.schilperoort@lumc.nl
**Corresponding author. Tel: +44-24-76-968585. E-mail: m.christian@warwick.ac.uk

attractive target to combat obesity and related disorders. Therefore, novel targets to increase BAT activity are highly warranted.

A potential target is G protein-coupled receptor 120 (GPR120), also termed free FA receptor 4 (FFAR4). We have previously shown that GPR120 is highly expressed in BAT and cold exposure further increases its expression in both BAT and subcutaneous WAT of mice (Rosell *et al*, 2014), suggesting that GPR120 contributes to the thermogenic capacity of BAT. GPR120 is activated by both medium-chain FA (MCFA) and long-chain FA (LCFAs) (Hirasawa *et al*, 2005; Christiansen *et al*, 2015) and is coupled to Gαq, which activates several intracellular signaling pathways. Recent studies have revealed that through these signaling mechanisms, GPR120 plays an important role in energy metabolism, hormonal regulation, and the immune system. For example, Oh *et al* (2010) demonstrate that GPR120 mediates the anti-inflammatory actions of ω-3 FAs. GPR120 deficiency leads to obesity, glucose intolerance, and hepatic steatosis in mice fed a high-fat diet (Ichimura *et al*, 2012). In humans, *GPR120* expression is higher in obese compared to lean subjects, and individuals carrying a mutation associated with decreased GPR120 signaling have an increased risk of obesity (Ichimura *et al*, 2012). Given the high GPR120 expression in BAT, it is likely that BAT contributes to the metabolic effects of GPR120 observed in these studies. Indeed, a very recent study by Quesada-López *et al* (2016) confirmed a role for GPR120 in BAT activation. However, therapeutic potential and underlying signaling of GPR120-mediated BAT activation remain to be elucidated.

Therefore, the aims of this study were to further investigate the therapeutic potential of GPR120 agonism and to address GPR120-mediated intracellular signaling in BAT. We found that stimulation of GPR120 by the agonist TUG-891 increases fat oxidation and lipid uptake by BAT thereby reducing fat mass, while GPR120 deficiency reduces expression of genes involved in nutrient handling. Mechanistically, we show that TUG-891 acts in a GPR120-dependent manner to induce intracellular Ca^{2+} release which could result in mitochondrial depolarization and fragmentation. In addition, our data reveal that TUG-891 activates mitochondrial UCP1, which may act synergistically with mitochondrial fragmentation to increase respiration. Taken together, our data indicate that by acutely increasing lipid combustion by BAT, GPR120 agonism may be a promising therapeutic strategy to reduce obesity.

Results

The GPR120 agonist TUG-891 increases lipid oxidation and reduces fat mass in mice

To investigate the effect of GPR120 activation on energy metabolism *in vivo*, mice were injected with the GPR120 agonist TUG-891 daily for a period of 2.5 weeks. This compound was selected due to higher selectivity for GPR120 over GPR40 compared to other agonists, including GW9508 and NCG21 (Shimpukade *et al*, 2012; Hudson *et al*, 2013). TUG-891 reduced total body weight (Fig 1A), which was due to a large reduction in fat mass (−73%; Fig 1B) and a minor reduction in lean mass (−9.9%; Fig 1C) at week 2.5 compared to vehicle. The reduced lean mass could be due to increased muscle turnover, as TUG-891 non-significantly increased expression of markers for both muscle atrophy and regeneration (Appendix Fig S1). During the first week of treatment, food intake was similar in the control and treatment groups (Fig 1D), while fat mass was already reduced by 19% in the TUG-891-treated group at day 5. Longer treatment reduced food intake, which further contributed to body weight and fat mass loss. To investigate whether TUG-891 enhances EE or alters substrate utilization, mice were housed in metabolic cages during the first week of treatment. TUG-891 treatment did not increase total EE (Appendix Fig S2A) nor did it affect physical activity levels (Appendix Fig S2B). However, TUG-891 acutely lowered the respiratory exchange ratio (RER) upon injection, which persisted throughout the dark period (Fig 1E). Accordingly, TUG-891 lowered glucose oxidation (Fig 1F) and largely increased fat oxidation (Fig 1G). This increase in fat oxidation was supported by histological analysis of adipose tissues, revealing that TUG-891 administration reduced lipid content in BAT (−28%; Fig 2A), and adipocyte size in both sWAT (−47%; Fig 2B) and gWAT (−38%; Fig 2C). In addition, total organ weights of iBAT (−31%), gWAT (−44%), and liver (−14%) were reduced in TUG-891-treated mice as compared to controls (Fig 2D). Plasma TG levels were increased at the end of the study, possibly as a result of increased lipolysis (Appendix Fig S3A). Protein (Appendix Fig S3B–E) and gene (Appendix Fig S3F) expressions of markers for lipolysis, adipogenesis, proliferation, and thermogenesis were largely unaffected in BAT. However, *Ucp1* gene expression (Appendix Fig S3H) and protein staining (Appendix Fig S4) were increased in gWAT of TUG-891-treated animals, suggesting GPR120-mediated browning.

As TUG-891 also has affinity for GPR40 (Hudson *et al*, 2013), we aimed to confirm that the effects of TUG-891 on body composition and substrate utilization were mediated by GPR120. To this end, metabolic effects of TUG-891 were also assessed in GPR120 KO mice and WT littermates. In GPR120 KO mice, TUG-891 non-significantly reduced body weight (Fig 3A) and fat mass (Fig 3B), but not to the same extent as in WT mice. TUG-891 decreased food intake similarly in WT and GPR120 KO mice (Fig 3C). The modest decrease in fat mass in TUG-891 GPR120 KO mice compared to non-treated WT mice may be related to diminished food intake. Lean mass was unchanged in all treatment groups (Fig 3D). In addition, while RER and fat oxidation did not differ between WT and GPR120 KO mice at baseline (Appendix Fig S5), TUG-891 non-significantly ($P = 0.136$) decreased RER (Fig 3E) and increased fat oxidation (Fig 3F) during the dark period in WT mice but not in GPR120 KO mice.

The GPR120 agonist TUG-891 stimulates fatty acid uptake by BAT

Hereafter, we aimed to elucidate which organs were responsible for the increased fat oxidation in TUG-891-treated WT animals. As increased fat oxidation subsequently leads to increased FA uptake, the tissue-specific uptake of FAs derived from intravenously injected lipoprotein-like particles labeled with glycerol tri[^{3}H]oleate was determined. In WT mice, TUG-891 treatment markedly increased the uptake of [^{3}H]oleate in both iBAT and subscapular BAT (sBAT) as compared to vehicle (Fig 4A), suggesting increased BAT activity. TUG-891 also increased the uptake of [^{14}C]deoxyglucose in iBAT and sBAT (Fig 4B). However, when the uptake data were corrected for organ weight (for organs that could be removed quantitatively within an acceptable time frame), the difference in glucose uptake was lost. FA uptake in whole iBAT remained approximately twice as high in treated WT mice versus controls (Appendix Fig S6),

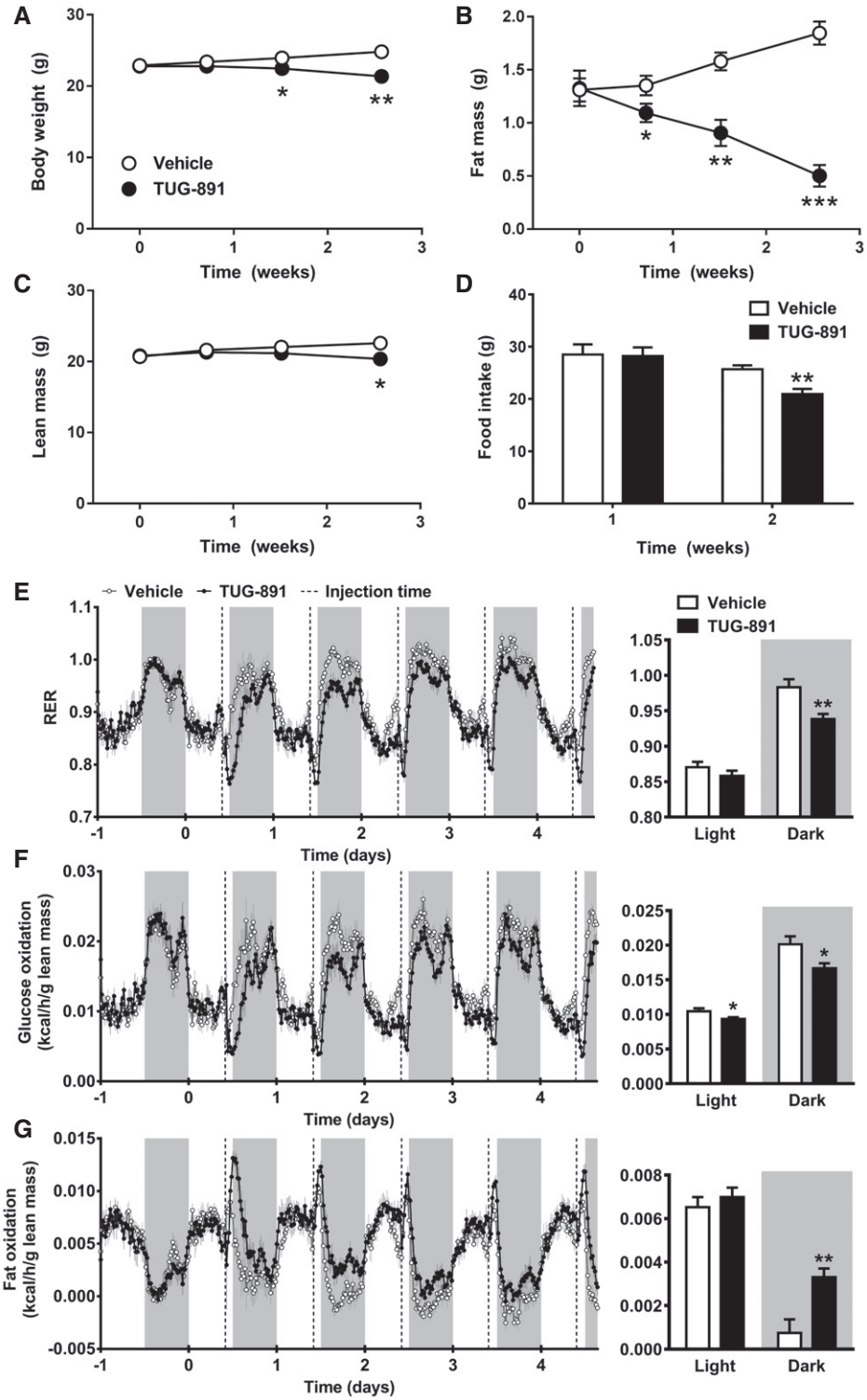

Figure 1. The GPR120 agonist TUG-891 decreases body weight and fat mass, and increases fat oxidation.

A–D C57Bl/6J mice on chow diet were treated with the GPR120 agonist TUG-891 (35 mg/kg) or vehicle (n = 8) for 2.5 weeks. Body weight, fat mass, lean mass, and food intake were measured at indicated time points.

E–G Vehicle- and TUG-891-treated mice (n = 8) were housed in fully automated metabolic cages in which respiratory exchange ratio (RER) (E), glucose oxidation (F), and fat oxidation (G) were measured. Injection of the GPR120 agonist TUG-891 (35 mg/kg) or vehicle is indicated by dotted lines, and light and gray areas represent the light and dark phase, respectively. For bar graph analysis, mean results in light and dark phase were calculated.

Data information: Data represent means ± SEM. *P < 0.05, **P < 0.01, ***P < 0.001 compared to the vehicle group, according to the two-tailed unpaired Student's t-test. The exact P-value for each significant difference can be found in Appendix Table S5.

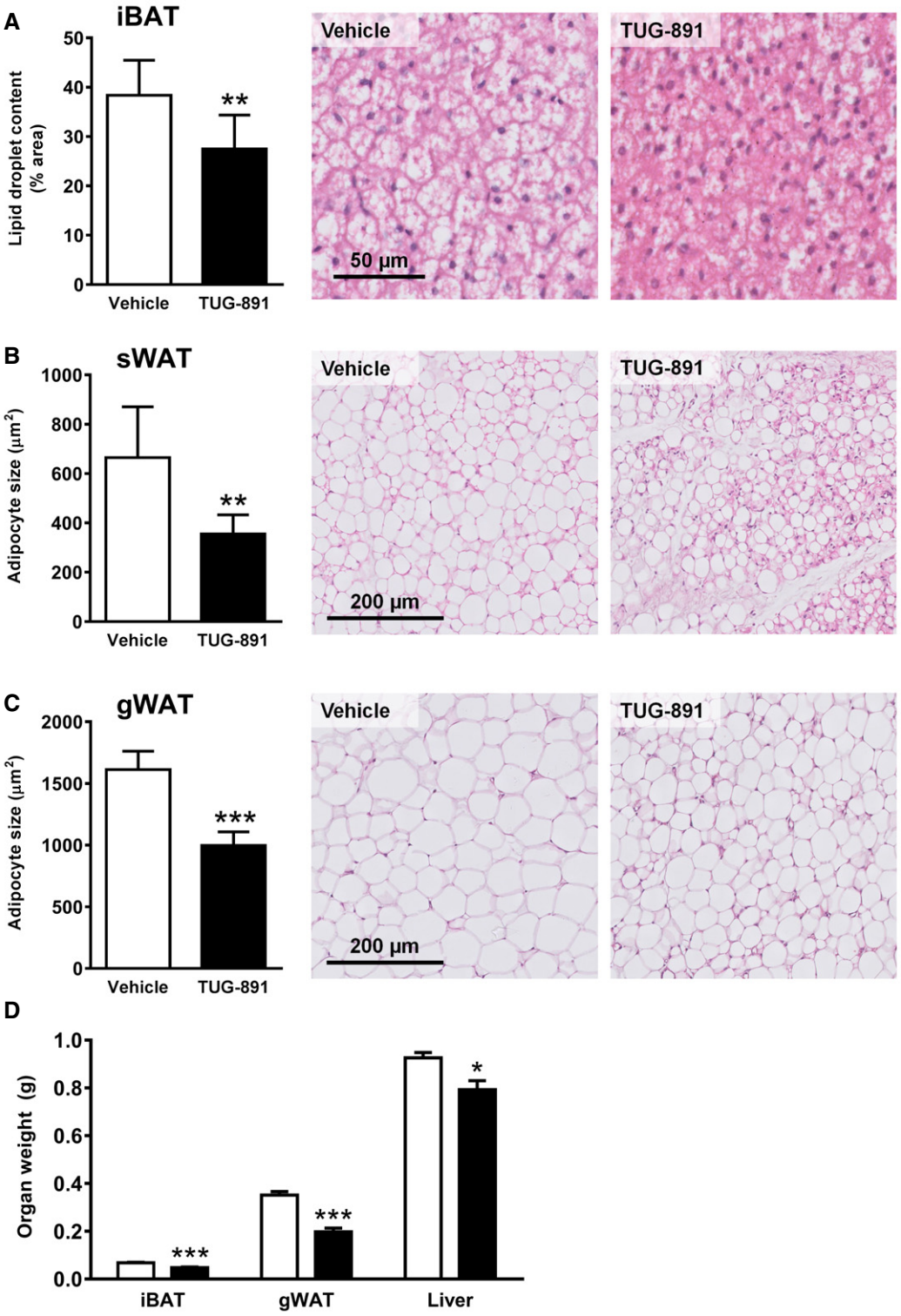

Figure 2. TUG-891 decreases lipid content of BAT and WAT.

A–C Representative images of hematoxylin and eosin (H&E)-stained interscapular BAT (iBAT), subcutaneous WAT (sWAT), and gonadal WAT (gWAT) of mice treated with vehicle or the GPR120 agonist TUG-891 (n = 8). Stained slides were digitalized, and lipid droplet content of BAT and adipocyte size in WAT was analyzed using ImageJ software.

D After mice treated with vehicle or the GPR120 agonist TUG-891 (n = 8) were sacrificed, iBAT, gWAT, and liver were collected and weighed (n = 8).

Data information: Data represent means ± SEM. *P < 0.05, **P < 0.01, ***P < 0.001 compared to the vehicle group, according to the two-tailed unpaired Student's t-test. The exact P-value for each significant difference can be found in Appendix Table S5.

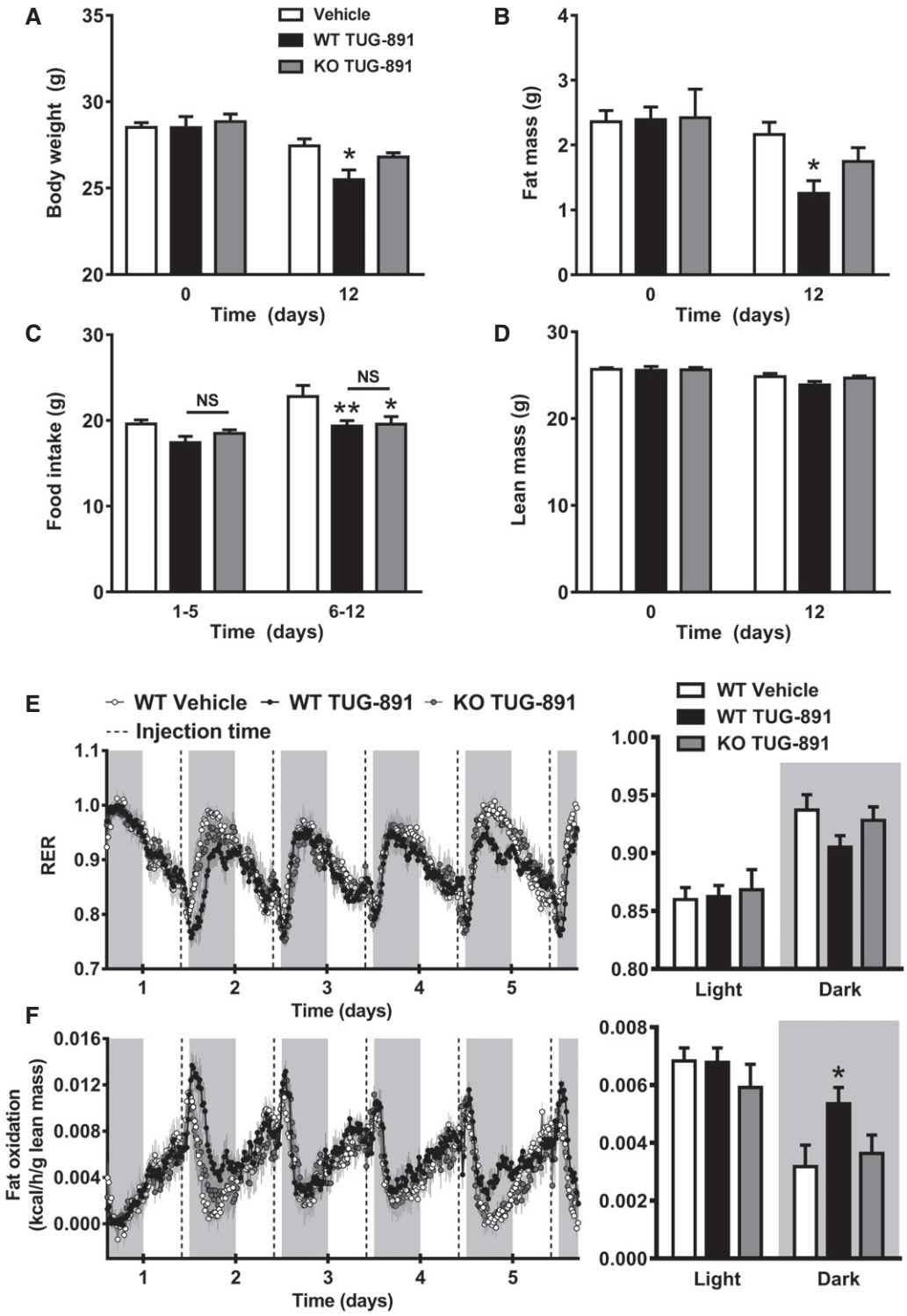

Figure 3. Metabolic effects of TUG-891 are reduced or absent in GPR120-deficient mice.

A–D GPR120 KO mice and WT littermates (n = 6–8) were treated with the GPR120 agonist TUG-891 (35 mg/kg) or vehicle for 12 days. At the beginning (day 0) and end (day 12) of this treatment period, body weight, fat mass, and lean mass were measured. Food intake was determined after 5 and 12 days of treatment.

E–F GPR120 KO mice and WT littermates (n = 6–8) were treated with the GPR120 agonist TUG-891 (35 mg/kg) or vehicle. Respiratory exchange ratio (RER) and fat oxidation were determined by housing the mice in metabolic cages. Injection of TUG-891 or vehicle is indicated by dotted lines, and light and gray areas represent the light and dark phase, respectively. For bar graph analysis, mean results in the light and dark phase were calculated.

Data information: Data represent means ± SEM. *$P < 0.05$, **$P < 0.01$ compared to the vehicle group, according to two-way ANOVA with Tukey's *post hoc* test. The exact P-value for each significant difference can be found in Appendix Table S5.

showing an independency of organ weight. In line with these data, TUG-891 decreased total organ weights of iBAT and sWAT depots as compared to vehicle in WT mice, but not in GPR120 KO mice (Fig 4C).

GPR120 alters expression of genes involved in nutrient handling

To evaluate how GPR120 modulates lipid handling by BAT, we investigated the effects of GPR120 deficiency on the global gene expression profile in BAT by performing a microarray on BAT of GPR120 KO and WT littermates. Clustering of genes was observed between GPR120 KO and WT mice (Fig 5A). The top 50 of genes that were either upregulated or downregulated in the absence of GPR120 are listed in Appendix Table S3. Selected genes were validated, and expression of genes associated with inflammation (Fig 5B), adipocyte biology (Fig 5C), glucose metabolism (Fig 5D), and lipid metabolism (Fig 5E) was investigated by qRT–PCR. Expression of inflammatory genes tended to be increased in GPR120 KO BAT. GPR120 deficiency upregulated *Sncg*, encoding synuclein-γ which is involved in lipid droplet dynamics in white adipocytes and is negatively regulated by PPARγ (Dunn *et al*, 2015). On the other hand, GPR120 deficiency downregulated *Mlxipl*, which encodes the carbohydrate response element-binding protein (ChREBP), a transcriptional inducer of glucose metabolism and *de novo* lipogenesis (Witte *et al*, 2015). Of the genes associated with glucose metabolism, *Glut4*, *Insr*, *Adcy4*, and *Gys2* were downregulated in GPR120 KO BAT. *Gys2* encodes glycogen synthase 2 and is PPARγ-regulated in adipocytes (Mandard *et al*, 2007). Of the genes that determine lipid metabolism, those involved in both lipogenesis (*Acc1*, *Acc2*, *Fas*, *Scd2*) and intracellular lipolysis (*Hsl*, *Atgl*, *Pnpla3*) were lower in GPR120 KO BAT.

Functional annotation clustering using DAVID (https://david.ncifcrf.gov/) (Dennis *et al*, 2003) revealed that genes downregulated in the absence of GPR120 were associated with mitochondrial function, FA metabolism, nucleotide binding, and mRNA processing (Appendix Table S4). The set of upregulated genes was associated with immune responses, as well as antigen processing and ribosomes.

Gpr120 expression promotes brown adipocyte differentiation and is increased in "browned" white adipocytes

Using a conditionally immortalized model of brown adipocytes (Rosell *et al*, 2014), we investigated the expression profile of *Gpr120* in preadipocytes differentiated to fully mature adipocytes over 7 days. Like *Ucp1* expression, *Gpr120* expression was highly induced during differentiation of brown adipocytes, reaching maximum levels on day 6 (Fig 6A). This is consistent with high GPR120 expression in BAT compared to other organs (Appendix Fig S7). Treatment of differentiated adipocytes with the β3-adrenergic agonist CL induced both *Gpr120* (ninefold) and *Ucp1* (53-fold) expression (Fig 6A). Differentiation also increased expression of adipocyte markers *aP2*, *Cidea*, and *Adrb3*, and decreased expression of the preadipocytes marker *Pref1*, validating our brown adipocyte cell line (Appendix Fig S8).

As we previously reported that *Gpr120* was induced by cold exposure in white adipose tissue (Rosell *et al*, 2014), we next investigated whether *in vitro* browning of white adipocytes with rosiglitazone treatment (resulting in so called "brite" adipocytes) could similarly enhance gene expression. Unlike *Ucp1* that was induced by CL in brown, white, and brite adipocytes, *Gpr120* expression was not increased by CL treatment in white and brite adipocytes (Fig 6B). However, basal expression of *Gpr120* in differentiated brite adipocytes was increased as compared to white adipocytes, indicating a potential role of *Gpr120* in browning of white adipocytes.

To study whether GPR120 is directly involved in adipocyte differentiation, brown adipocyte cell lines were generated from WT and GPR120 KO mice. Both cell lines differentiated to mature brown adipocytes when exposed to a standard hormone differentiation treatment. However, GPR120 KO adipocytes accumulated a lower amount of lipids as evidenced by Oil Red O staining (Fig 6C) and exhibited lower expression of the adipocyte differentiation marker *aP2* and *Ucp1* (Fig 6D), suggesting impaired differentiation in GPR120 KO cells. Treatment with TUG-891 throughout differentiation tended to increase *Ucp1* expression in WT but not GPR120 KO cells (Fig 6D).

TUG-891 directly activates brown adipocytes *in vitro* through UCP1 activation and mitochondrial fragmentation

To investigate whether the GPR120 agonist TUG-891 directly activates brown adipocytes and to study the downstream intracellular signaling pathways involved, we stimulated differentiated brown adipocytes with TUG-891. Strikingly, TUG-891 acutely increased the O_2 consumption rate (OCR) of brown adipocytes by more than twofold (Fig 7A). Pretreatment with the GPR120 antagonist AH7614 reduced rather than abolished this response (Fig 7A), indicating that TUG-891 exhibits both GPR120-dependent and GPR120-independent activity. We investigated whether TUG-891 functions in a manner similar to LCFAs which can directly activate UCP1 by measuring O_2 consumption in isolated BAT mitochondria in conditions mimicking a cellular environment with high purine nucleotide (GDP) content and inhibited UCP1 (Matthias *et al*, 2000). Indeed, TUG-891 ($\geq$ 10 μM) increased O_2 consumption in mitochondria isolated from WT mice (Fig 7B), suggesting that TUG-891 has the capacity to overcome purine nucleotide inhibition and activate UCP1 in brown adipocytes. TUG-891 also increased O_2 consumption in mitochondria from UCP1 KO mice, but this effect was smaller and occurred at higher concentrations ($\geq$ 90 μM) as compared to WT mitochondria (Fig 7C), a response that is also observed with oleate (Shabalina *et al*, 2004). As oxidative capacity (FCCP response, Fig 7B and C) of WT and UCP1 KO mitochondria was equal, these results suggest that TUG-891 increases mitochondrial respiration through activation of UCP1 (Appendix Fig S9A). TUG-891 exhibited a competitive interaction with GDP in WT but not UCP1 KO mitochondria (Appendix Fig S9B and C), further supporting the effect of TUG-891 on UCP1.

Next, we investigated GPR120-dependent effects of TUG-891 by examining potential downstream targets of G protein signaling that could partly mediate the TUG-891-induced O_2 consumption in brown adipocytes. To ensure that GPR120 is Gαq-coupled and does not signal via Gαs in brown adipocytes, the effect of TUG-891 on intracellular cAMP levels was determined. As expected, TUG-891 had no effect on cAMP production (Appendix Fig S9D). As for Gαq targets, TUG-891 increased the amount of phosphorylated ERK and AKT (Appendix Fig S9E). However, pretreatment of brown

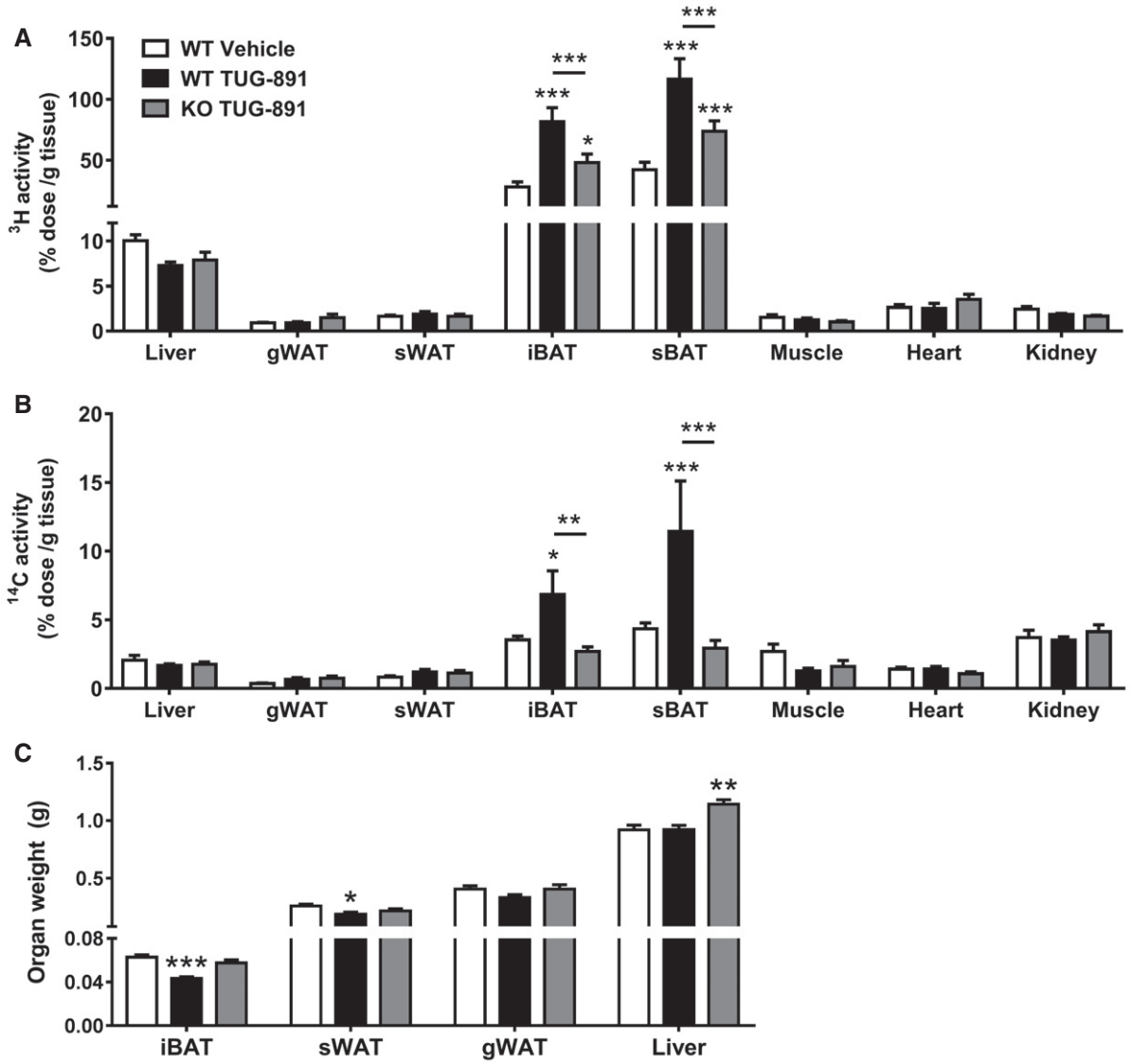

Figure 4. TUG-891 increases the uptake of nutrients by BAT.

A, B WT and GPR120 KO mice (n = 6–8) treated with vehicle or the GPR120 agonist TUG-891 were intravenously injected with [^{3}H]TO-labeled lipoprotein-like emulsion particles and [^{14}C]deoxyglucose ([^{14}C]DG). After 15 min, mice were sacrificed and uptake of [^{3}H]TO- and [^{14}C]DG-derived radioactivity per gram tissue was determined in various organs, including gonadal WAT (gWAT), subcutaneous WAT (sWAT), interscapular BAT (iBAT), and subscapular BAT (sBAT).

C After WT and GPR120 KO mice (n = 6–8) treated with vehicle or the GPR120 agonist TUG-891 were sacrificed, organs were collected and weighed.

Data information: Data represent means ± SEM. *P < 0.05, **P < 0.01, ***P < 0.001 compared to the vehicle group or indicated control group, according to two-way ANOVA with Tukey's *post hoc* test (A, B) or the two-tailed unpaired Student's t-test (C). The exact P-value for each significant difference can be found in Appendix Table S5.

adipocytes with the MEK inhibitor U0126 (Appendix Fig S9F) or an AKT 1/2 kinase inhibitor (Appendix Fig S9G) did not reduce O_2 consumption, excluding requirement of the ERK and AKT pathways for this effect. Pretreatment with the cell-permeable Ca^{2+} chelator BAPTA-AM strongly reduced the TUG-891-induced O_2 consumption (Fig 7D), indicating that intracellular Ca^{2+} is essential for GPR120-mediated activation of brown adipocytes. Indeed, TUG-891 strongly increased intracellular Ca^{2+} concentrations (Fig 7E). This effect was absent in adipocytes preincubated with the GPR120 antagonist AH7614 and in GPR120 KO adipocytes (Fig 7E), confirming GPR120 dependency. The Gαq inhibitor YM-254890 also blocked the Ca^{2+} response (Appendix Fig S9H), indicating that this effect of GPR120 activation is indeed mediated via Gαq signaling. As Ca^{2+} could affect mitochondrial polarization, effects of TUG-891 on mitochondrial membrane potential were investigated. Cells were incubated with MitoTracker Green FM (MTG) and MitoTracker Red CMXRos (MTR), which stain mitochondria independent of and dependent on membrane potential, respectively. Relative intensity (MTR/MTG) of these stainings can be used as a measure for mitochondrial polarization. Stimulation with TUG-891 resulted in fading of the MTR signal

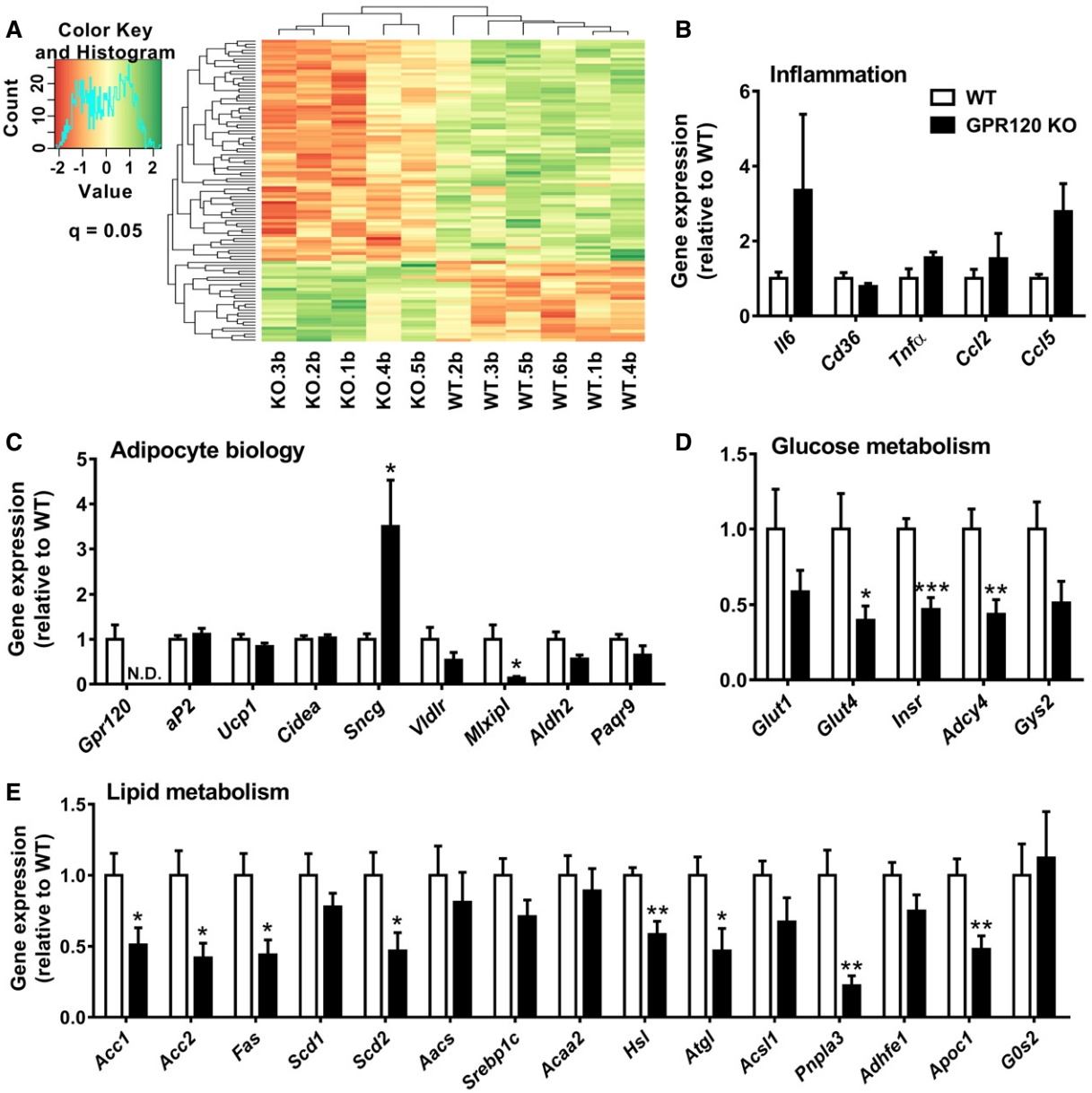

Figure 5. GPR120 deficiency alters the expression of genes involved in glucose and lipid metabolism in BAT.

A Probe sets for WT and GPR120 KO BAT from microarray analysis are colored according to average expression levels across all samples, with green denoting a higher expression level and red denoting a lower expression level. The probe sets shown in the heat map passed the threshold of absolute value of the logFC > 0.5 and *P*-adjusted < 0.05.

B–E Expression of genes involved in inflammation, adipocyte biology, glucose metabolism, and lipid metabolism in BAT from GPR120 KO mice (n = 5) and WT littermates (n = 6) was determined through qRT–PCR (N.D. = non-detectable). Data represent means ± SEM. *P < 0.05, **P < 0.01, ***P < 0.001 compared to the WT control group, according to the two-tailed unpaired Student's t-test. The exact P-value for each significant difference can be found in Appendix Table S5.

while the MTG signal remained intense, indicative of mitochondrial depolarization (Fig 7F). In addition, mitochondria were more fragmented following TUG-891 stimulation (Fig 7G), pointing toward increased mitochondrial fission, which could explain the GPR120-dependent increase in respiration. Of note, the timing of TUG-891-induced changes in mitochondrial morphology coincides with increases in intracellular Ca^{2+}, suggesting this effect is mediated through Ca^{2+}.

Discussion

In the current study, we aimed to investigate the therapeutic potential and mechanism of action of GPR120 agonism. We specifically focussed on BAT and demonstrated that the GPR120 agonist TUG-891 increases the activity of brown adipocytes, potentially by stimulating Ca^{2+}-induced mitochondrial depolarization and fission. In addition, TUG-891 may act GPR120 independently to activate UCP1

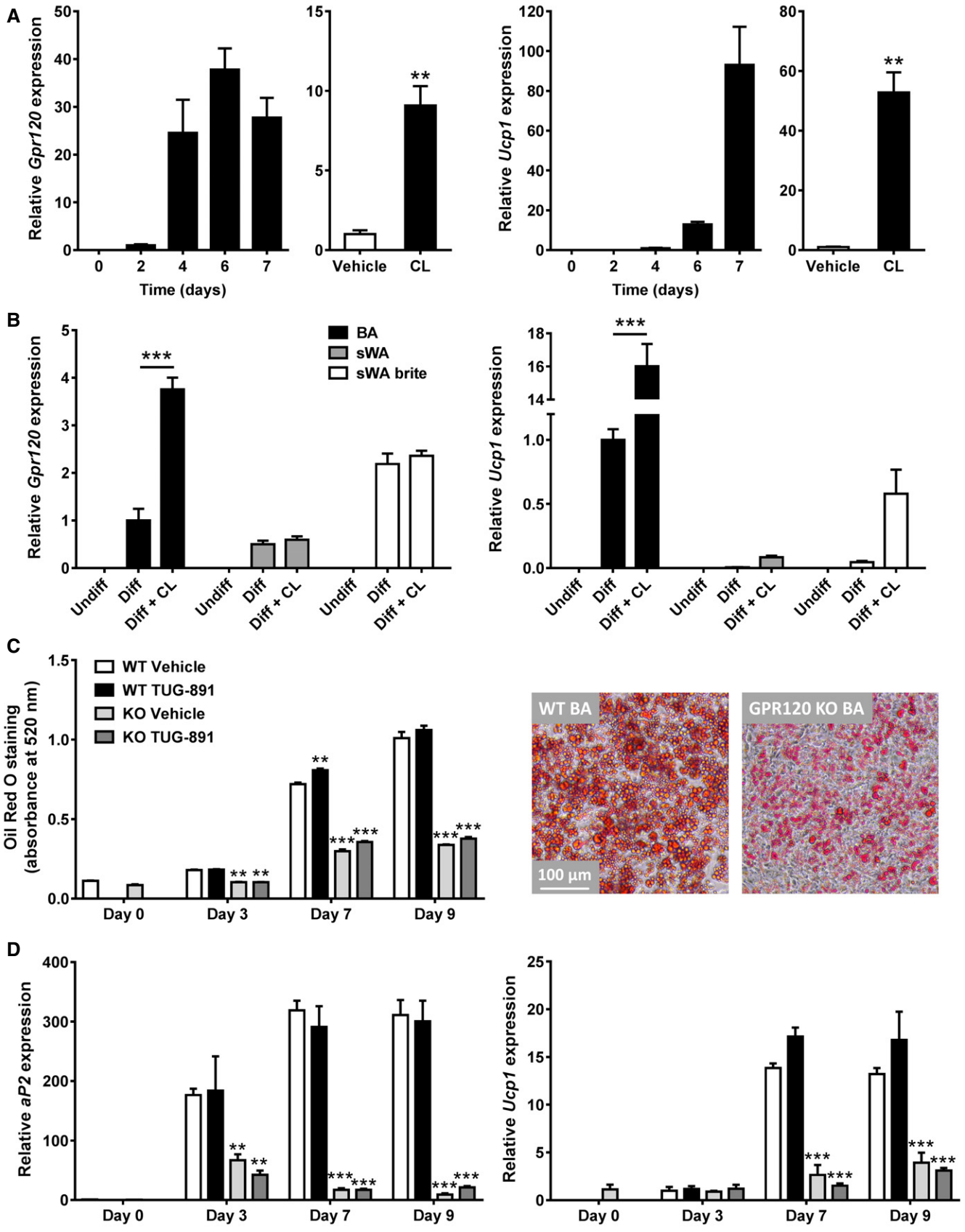
A
Relative Gpr120 expression
Time (days)
Vehicle
CL
Relative Ucp1 expression
B
BA
sWA
sWA brite
Undiff
Diff
Diff + CL
C
WT Vehicle
WT TUG-891
KO Vehicle
KO TUG-891
Oil Red O staining (absorbance at 520 nm)
Day 0
Day 3
Day 7
Day 9
WT BA
GPR120 KO BA
100 µm
D
Relative aP2 expression

Figure 6.

Figure 6. GPR120 is involved in differentiation of brown adipocytes and browning of white adipocytes.

A Immortalized murine brown adipocytes (n = 3) were differentiated for 0, 2, 4, 6, or 7 days after which expression of *Gpr120* and *Ucp1* was determined by qRT–PCR. On day 7, a subset of adipocytes (n = 3) was stimulated with CL (10 μM) or vehicle.

B Expression of *Gpr120* and *Ucp1* was measured in undifferentiated (Undiff), differentiated (Diff), and CL-treated (Diff + CL) brown adipocytes (BA), subcutaneous white adipocytes (sWA), and sWA treated with the browning agent rosiglitazone (sWA brite) (n = 3).

C WT and GPR120 KO brown adipocytes (n = 3) were treated with vehicle or TUG-891 (10 μM) throughout differentiation and stained at day 0, 3, 7, and 9 of differentiation with Oil Red O. Absorbance of the staining at 520 nm was quantified. A representative image at day 8 of differentiation was taken with a phase-contrast microscope (Leica) at 20-fold magnification.

D As in (C), WT and GPR120 KO brown adipocytes (n = 3) were treated with vehicle or TUG-891 throughout differentiation to analyze expression patterns of *aP2* and *Ucp1*.

Data information: Data represent means ± SEM. $^{**}P < 0.01$ compared to the vehicle group, $^{***}P < 0.001$ compared to the WT control group or indicated controls, according to the two-tailed unpaired Student's *t*-test (A) or two-way ANOVA with Dunnett's *post hoc* test (B–D). The exact *P*-value for each significant difference can be found in Appendix Table S5.

and increase uncoupled respiration. These mechanisms could have acted synergistically *in vivo* to induce BAT activation, thereby increasing lipid oxidation and reducing fat mass.

We assessed the therapeutic potential of GPR120 activation by using the agonist TUG-891, a more selective and potent agonist for GPR120 than α-linolenic acid, GW9508, and NCG21 (Shimpukade *et al*, 2012; Hudson *et al*, 2013). Mice treated with TUG-891 exhibited decreased body weight and fat mass, and an increased fat oxidation. These results are in line with a previous study that observed reduced body weight after chronic GPR120 agonist treatment in diet-induced obese mice (Azevedo *et al*, 2016). The increased fat oxidation upon TUG-891 treatment suggested involvement of BAT, as previous studies have demonstrated that selective BAT activation specifically stimulates lipid oxidation (Berbee *et al*, 2015; Schilperoort *et al*, 2016). Indeed, TUG-891 enhanced the uptake of TG-derived FA by BAT, indicating an increased lipid combustion in BAT resulting in a higher need to take up lipids from the circulation. Moreover, lipid droplet content in iBAT and total iBAT weight were decreased in TUG-891-treated mice, also a feature of increased BAT activity. Adipocyte size was decreased in WAT of TUG-891-treated mice, indicative of increased lipolysis in WAT, possibly to release lipids into the circulation to fuel the highly active BAT.

To further elucidate the importance of GPR120 for BAT functionality, we examined expression patterns of *Gpr120 in vivo* and *in vitro*. We found that *Gpr120* is highly expressed in BAT as compared to other tissues. Furthermore, *Gpr120* expression increased during brown adipocyte differentiation and upon treatment with the classical BAT activator CL (Berbee *et al*, 2015). This is in line with previous data showing that cold exposure, the most potent browning stimulus, increases the expression of *Gpr120* in BAT, sWAT, and gWAT (Rosell *et al*, 2014). Rosiglitazone, a PPARγ agonist that stimulates browning (Ohno *et al*, 2012), induced *Gpr120* expression in subcutaneous white adipocytes *in vitro*. A similar effect of browning on *Gpr120* expression was observed earlier upon treatment of 3T3-L1 white adipocytes with the PPAR agonist troglitazone (Gotoh *et al*, 2007). These results demonstrate that like *Ucp1*, *Gpr120* is highly expressed in brown adipocytes and increases during differentiation and browning, signifying an important role for *Gpr120* in BAT physiology. This is further supported by reduced lipid accumulation and *aP2* expression in GPR120-deficient adipocytes, indicative of impaired differentiation. The latter findings concur with previous studies that used siRNA to knockdown *Gpr120* expression in 3T3-L1 cells, which resulted in reduced lipid droplet accumulation and *aP2* expression (Gotoh *et al*, 2007; Liu *et al*, 2012). The expression of genes involved in glucose and lipid metabolism was reduced in BAT from GPR120-deficient mice, suggesting that the uptake and handling of nutrients are less efficient in the absence of GPR120. This is in accordance with the increased uptake of nutrients by BAT upon GPR120 stimulation by TUG-891.

Our findings that expression of *Gpr120* in BAT was highest as compared to other organs and that *Gpr120* expression is induced upon brown adipocyte differentiation were corroborated by

Figure 7. TUG-891 increases oxygen consumption by brown adipocytes, mediated by direct UCP1 activation and mitochondrial fragmentation.

A Immortalized brown adipocyte (n = 5–6) was pretreated with either vehicle or the GPR120 antagonist AH7614 (100 μM) for 30 min, followed by measurement of the basal oxygen consumption rate (OCR) for 15 min in a Seahorse XF24 analyzer. Hereafter, cells were treated with either vehicle or the GPR120 agonist TUG-891 (10 μM) and OCR was measured for another 30 min.

B, C Representative traces showing the effects of TUG-891 (heavy line) and vehicle (thin line) on oxygen consumption in BAT mitochondria (0.125 mg/ml) from WT (B) and UCP1 KO (C) mice (n = 4–5). Additions were mitochondria (M), GDP (1 mM), TUG-891 (successively added in the concentration range of 10–150 μM), and FCCP (1.0–1.4 μM). The breaks in trace indicate periods of chamber re-oxygenation.

D Immortalized brown adipocytes (n = 5–6) were pretreated for 30 min with vehicle or BAPTA-AM (25 μM), after which the OCR was determined in a Seahorse XF24 analyzer. After three baseline measurements, either vehicle or TUG-891 (10 μM) was injected into the wells.

E WT and GPR120 KO brown adipocytes were incubated with the calcium-sensitive dye Fluo-4-AM for 1 h at RT, followed by live cell imaging with a confocal laser scanning microscope (LSM 510, Zeiss) and stimulation with TUG-891 (10 μM) with or without the presence of AH7614 (100 μM). F_1/F_0 represents peak fluorescence divided by baseline fluorescence.

F Representative images of a brown adipocyte stained with MitoTracker Green FM (125 nM) and MitoTracker Red CMXRos (250 nM) before and after stimulation with TUG-891 (10 μM) for 10 min. Fluorescence intensity of MTR/MTG was determined in TUG-891-treated cells and controls (n = 8–9) at baseline and after 10 min of fluorescence imaging, and plotted relative to baseline.

G Representative images of a brown adipocyte stained with MitoTracker Green FM at baseline (0 min) and 2, 4, and 8 min after TUG-891 stimulation. MitoTracker-stained live cells were imaged using a confocal laser scanning microscope (Leica TCS SP8, Leica Microsystems).

Data information: Data represent means ± SEM. $^{**}P < 0.01$, $^{***}P < 0.001$ compared to the vehicle group, $^{\#}P < 0.05$ compared to the TUG-891 control group (or baseline in Fig 7F), according to the two-tailed unpaired Student's *t*-test. The exact *P*-value for each significant difference can be found in Appendix Table S5.

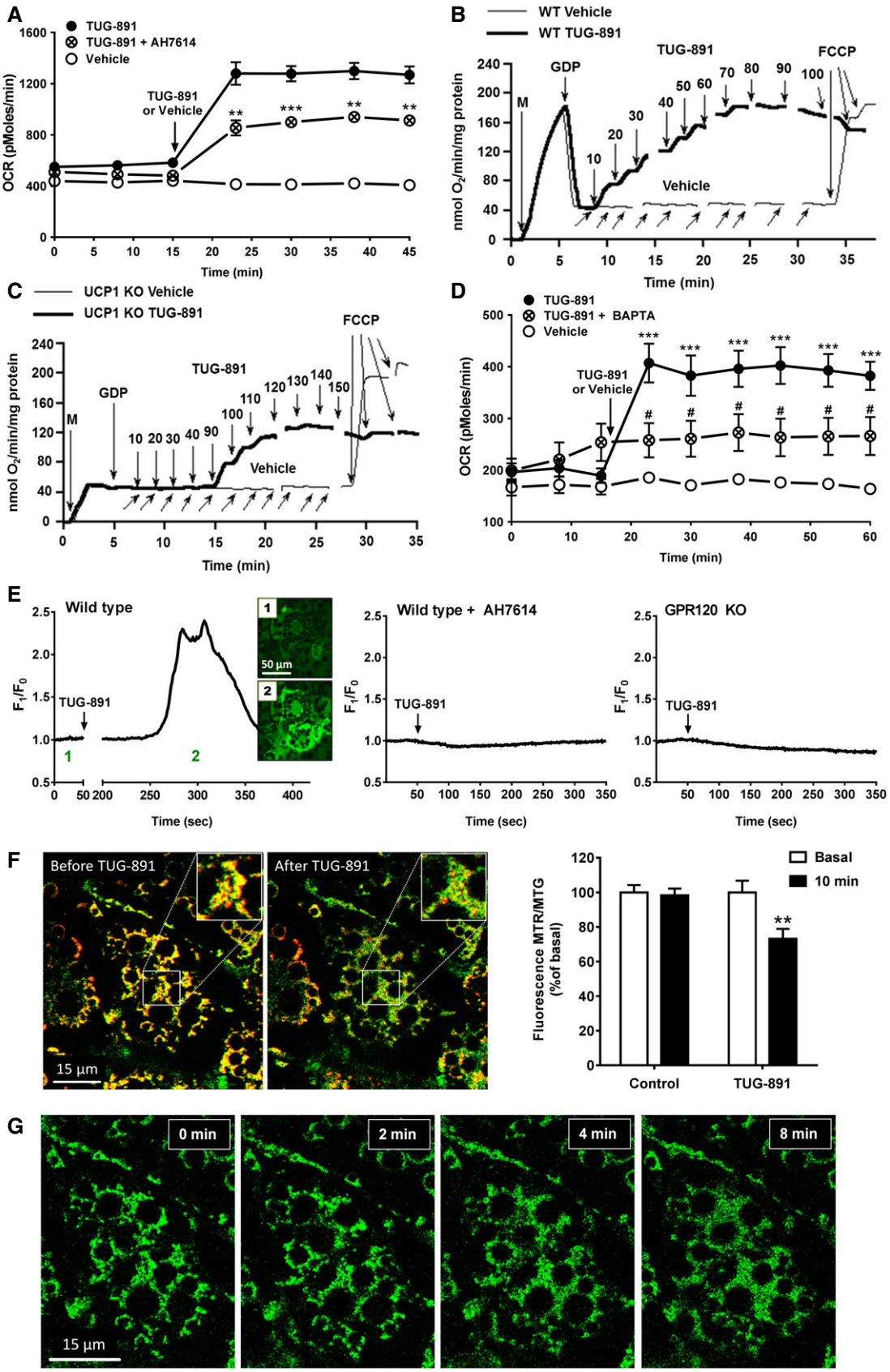
A
TUG-891
TUG-891 + AH7614
Vehicle
OCR (pMoles/min)
TUG-891 or Vehicle
Time (min)
B
WT Vehicle
WT TUG-891
nmol O2/min/mg protein
GDP
TUG-891
FCCP
Vehicle
Time (min)
C
UCP1 KO Vehicle
UCP1 KO TUG-891
nmol O2/min/mg protein
GDP
TUG-891
FCCP
Vehicle
Time (min)
D
TUG-891
TUG-891 + BAPTA
Vehicle
OCR (pMoles/min)
TUG-891 or Vehicle
Time (min)
E
Wild type
Wild type + AH7614
GPR120 KO
F1/F0
TUG-891
50 µm
Time (sec)
F
Before TUG-891
After TUG-891
15 µm
Fluorescence MTR/MTG (%of basal)
Basal
10 min
Control
TUG-891
G
0 min
2 min
4 min
8 min
15 µm

Figure 7.

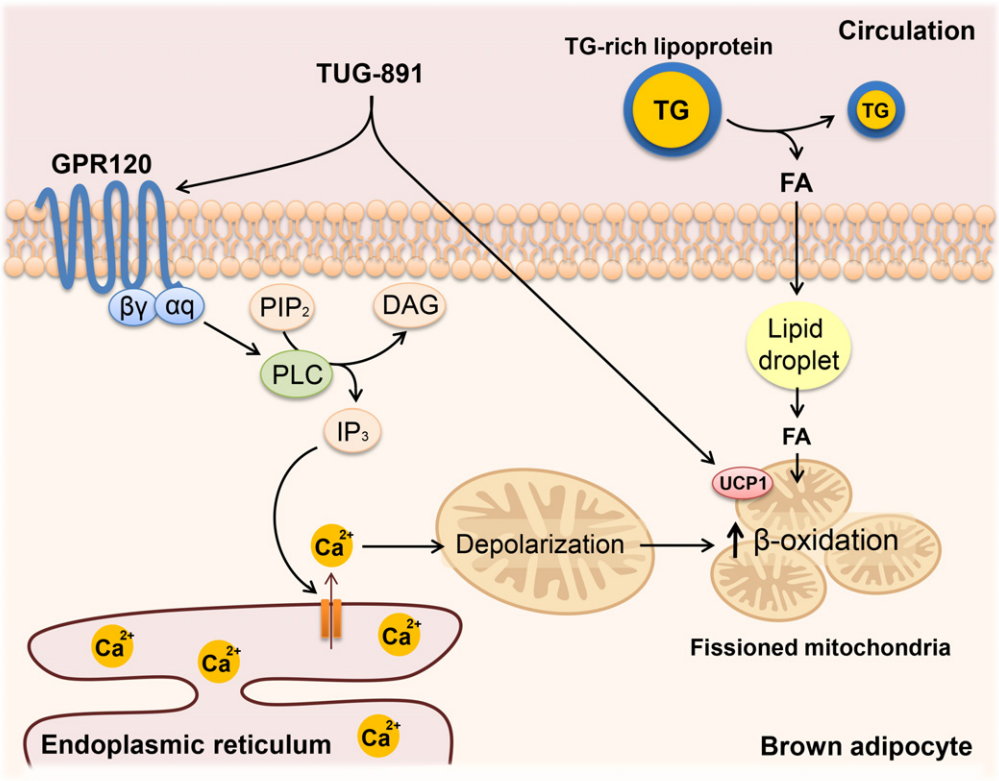

Figure 8. Proposed mechanism by which the GPR120 agonist TUG-891 activates BAT.

TUG-891 selectively agonizes the Gαq-coupled GPR120, which activates phospholipase C (PLC). Upon activation, PLC cleaves phospholipid phosphatidylinositol 4,5-bisphosphate (PIP2) into diacyl glycerol (DAG) and inositol trisphosphate (IP3). IP3 triggers the opening of Ca^{2+} channels in the membrane of the endoplasmic reticulum, thereby increasing intracellular Ca^{2+} concentrations. Increased Ca^{2+} leads to depolarization of the mitochondria, and subsequently induction of mitochondrial fission which increases respiration. In addition, TUG-891 directly activates UCP1, further stimulating uncoupled respiration and lipid combustion. As a consequence, the activated brown adipocytes take up fatty acids (FA) from triglyceride (TG)-rich lipoproteins from the circulation, which eventually reduces fat mass.

Quesada-López *et al* (2016). They showed that the GPR120 agonist GW9508 upregulated thermogenic genes in BAT and increased O_2 consumption in mice, without changes in body weight and food intake. However, GW9508 also increased O_2 consumption and UCP1 levels in GPR120 KO animals. Potentially, these effects of GW9508 are mediated through GPR40 (Ou *et al*, 2013), as GW9508 activates both GPR40 and GPR120 and is approximately 100-fold more selective for GPR40 than GPR120 (Briscoe *et al*, 2006). GPR40 is involved in insulin secretion and glucose metabolism (Itoh *et al*, 2003; El-Azzouny *et al*, 2014), and GPR40 KO mice develop obesity, glucose intolerance, and insulin resistance (Kebede *et al*, 2008). Also, activation of GPR40 has recently been shown to reduce food intake and body weight in mice (Gorski *et al*, 2017). In our study, food intake was reduced in both wild-type and GPR120 KO mice treated with TUG-891. Therefore, this effect might be mediated through GPR40 instead of GPR120. However, effects of TUG-891 on body weight, fat mass, and fat oxidation were reduced or absent in GPR120 KO mice, confirming that these beneficial metabolic effects of TUG-891 were predominately mediated through GPR120.

We next verified whether the BAT-activating effects of TUG-891 *in vivo* were a consequence of a direct effect of TUG-891 on brown adipocytes. In line with the acute effect of TUG-891 on the RER and fat oxidation *in vivo*, TUG-891 acutely increased O_2 consumption by brown adipocytes *in vitro*. This indicates that the effects of TUG-891 *in vivo* could all have been mediated by direct BAT activation. However, we cannot exclude involvement of other tissues, as GPR120 is not exclusively expressed on brown adipocytes. For example, GPR120 is expressed in the hypothalamus and central agonism of GPR120 has been shown to affect energy metabolism (Auguste *et al*, 2016; Dragano *et al*, 2017). However, as carboxylic acids similar to TUG-891 have difficulty penetrating the blood–brain barrier, this is not very likely (Pajouhesh & Lenz, 2005). Also, conflicting reports exist on whether GPR120 plays a role in muscle physiology and metabolism (Oh *et al*, 2010; Kim *et al*, 2015). In our study, expression of *Gadd45a*, *Murf1*, and *Myog* in skeletal muscle tissue was mildly affected by TUG-891 treatment. Whether this is an off-target effect or GPR120-mediated effect, which could affect muscle function, remains to be investigated. Future experiments with tissue-specific GPR120 KO mice would be valuable to assess tissue specificity of TUG-891. In addition, it would be interesting to repeat our *in vivo* experiments at thermoneutrality, to substantiate the link between BAT activation and the observed phenotype.

Using a GPR120 antagonist, we discovered that the TUG-891-induced increase in O_2 consumption in brown adipocytes is only

partly mediated by GPR120. The GPR120-independent effect of TUG-891 could be due to direct activation of mitochondrial UCP1. TUG-891 relieves the natural inhibition of UCP1 by GDP (Matthias *et al*, 2000), similar to oleate and other LCFAs (Shabalina *et al*, 2004; Fedorenko *et al*, 2012), thereby leading to increased UCP1 activity and uncoupled mitochondrial respiration. This could explain the moderately decreased fat mass and increased FA uptake by BAT in TUG-891-treated GPR120 KO mice. However, as most metabolic effects of TUG-891 were largely attenuated or abolished in GPR120 KO mice, BAT activation by TUG-891 *in vivo* is mainly dependent on GPR120 signaling.

To investigate through which mechanism GPR120 signaling could increase brown adipocyte activity, several Gαq-coupled signaling pathways were studied: the PI3K/AKT pathway, MAPK/ERK pathway, and signaling through Ca^{2+}. Of these, only the intracellular Ca^{2+} availability was proven to be essential for GPR120-mediated activation of brown adipocytes. A recent study showed that Ca^{2+} could increase respiration in brown adipocytes by decreasing the mitochondrial membrane potential (MMP) (Hou *et al*, 2017). Evidently, the β receptor agonist isoprenaline induces Ca^{2+} release from the endoplasmic reticulum of brown adipocytes resulting in mitochondrial depolarization and fission (Hou *et al*, 2017), the latter being a process required for NA-induced uncoupled respiration (Wikstrom *et al*, 2014). Therefore, we studied whether this Ca^{2+}-mediated pathway of mitochondrial depolarization and fission could also underlie GPR120-mediated activation of brown adipocytes. Mitochondria were co-stained with the MMP-sensitive MitoTracker CMXRos (MTR) and the MMP-insensitive MitoTracker Green (MTG) (Pendergrass *et al*, 2004), and the relative ratio of MTR/MTG was used as a measure for mitochondrial depolarization (as seen in (Wikstrom *et al*, 2014) in which TMRE was used instead of MTR. TUG-891 stimulation resulted in a reduction in the MTR/MTG ratio, indicative of mitochondrial depolarization. Also, TUG-891 increased mitochondrial fragmentation, presumably secondary to Ca^{2+}-induced mitochondrial depolarization. These results suggest that GPR120 signaling could increase metabolic activity of brown adipocytes by stimulation of mitochondrial fission in a Ca^{2+}-dependent manner.

We conclude that TUG-891, an agonist of the free FA receptor GPR120, directly stimulates BAT activity via both GPR120-dependent and GPR120-independent mechanisms (Fig 8). As a consequence, lipid uptake and oxidation by BAT increases, eventually reducing body weight and fat mass. Since impaired GPR120 signaling predisposes to obesity in humans (Ichimura *et al*, 2012), obese individuals could benefit from GPR120 activation. Although further studies are needed to investigate the safety of TUG-891 and the potential of GPR120 agonists to activate BAT in humans, we thus anticipate that GPR120 agonism is a promising therapeutic strategy to increase BAT activity, thereby increasing fat oxidation and reducing obesity.

Materials and Methods

Animals

To assess effects of TUG-891 on energy metabolism, 8- to 10-week-old male C57Bl/6J mice (Charles River Laboratories) were randomized to receive an intraperitoneal injection with either TUG-891 (35 mg/kg) or 10% dimethyl sulfoxide (DMSO) vehicle dissolved in PBS once daily for 2.5 weeks. TUG-891 was synthesized as previously described (Shimpukade *et al*, 2012) and was of > 99.5% purity, as assessed by HPLC and NMR. Mice were injected 2 h before initiation of the dark phase. To evaluate the specificity of TUG-891 for GPR120, this experiment was also performed in 10- to 14-week-old male GPR120 knockout (KO) mice and wild-type (WT) littermates on a C57Bl/6J background for a total period of 2 weeks. All mice were housed in conventional cages with a 12-h light/dark cycle and had *ad libitum* access to chow diet and water. Mouse experiments were performed in accordance with the Institute for Laboratory Animal Research Guide for the Care and Use of Laboratory Animals after having received approval from the University Ethical Review Board (Leiden University Medical Center, Leiden, The Netherlands).

To evaluate *Gpr120* gene expression in various tissues, 12-week-old FVB/N female mice were sacrificed by cervical dislocation and organs were collected. Mice were housed in conventional cages with a 12-h light/dark cycle and had *ad libitum* access to chow diet and water, and experiments were carried out in accordance with UK Home Office regulations.

For experiments in which mitochondrial respiration was measured, mitochondria were isolated from 8- to 10-week-old male UCP1 KO mice (progeny of those described in Enerback *et al*, 1997) backcrossed to C57Bl/6J mice and wild-type C57Bl/6J mice. Mice were housed in conventional cages with a 12-h light/dark cycle and had *ad libitum* access to chow diet and water, and experiments were carried out in accordance with the Animal Ethics Committee of the North Stockholm region in Sweden.

Food intake, body weight, and body composition measurements

At the indicated time points, food intake and body weight of mice were measured with a scale, and lean and fat mass with an EchoMRI-100-analyzer.

Indirect calorimetry

Indirect calorimetry was performed in fully automated metabolic cages (LabMaster System, TSE Systems) during the first week of treatment. After 3 days of acclimatization, O_2 consumption (VO_2), CO_2 production (VCO_2), and caloric intake were measured for 5 consecutive days. Total EE was estimated from the VO_2 and resting energy requirement. Carbohydrate oxidation was calculated using the formula $((4.585*VCO_2) - (3.226*VO_2))*4$, in which the 4 represents the conversion from mass per time unit to kcal per time unit (Peronnet & Massicotte, 1991). Similarly, fat oxidation was calculated using the formula $((1.695*VO_2) - (1.701*VCO_2))*9$. Physical activity was measured with infrared sensor frames.

Tissue histology and immunohistochemistry

Formalin-fixed interscapular BAT (iBAT), subcutaneous WAT (sWAT), and gonadal WAT (gWAT) were dehydrated in 70% EtOH, embedded in paraffin, and cut into 5-μm sections. Sections were stained with hematoxylin and eosin (H&E) using standard protocols. UCP1 staining was performed as previously described (Berbee *et al*, 2015). In short,

sections were treated with 3% H_2O_2 for 30 min and boiled in citrate buffer (10 mM, pH 6) for 10 min. Slides were blocked with 1.3% normal goat serum, incubated overnight at 4°C with rabbit monoclonal anti-UCP1 antibody (1:400, Abcam) followed by 1-h incubation with biotinylated goat α-rabbit secondary antibody (Vector Labs). Immunostaining was amplified using Vector Laboratories Elite ABC kit (Vector Labs) and visualized with Nova Red (Vector Labs). Counterstaining was performed with hematoxylin. All sections were digitalized with Philips Digital Pathology Solutions (PHILIPS Electronics) for morphological measurement. White adipocyte size, iBAT lipid droplet content, and UCP1 expression (relative UCP1 staining per area) were quantified using ImageJ software (Version 1.50).

Plasma triglycerides

After 6 h of food withdrawal, blood was collected from the tail vein in paraoxon-coated capillaries, and plasma levels of TG were determined using an enzymatic kit (Roche Diagnostics)

RNA isolation, cDNA synthesis, and qRT–PCR

Tissues or cells were dissolved in TRIzol RNA isolation reagent (Thermo Fisher) following the manufacturer's protocol. The RNA concentration was determined with a NanoDrop spectrophotometer (Thermo Fisher). For removal of genomic DNA, samples were treated with DNase I (Sigma), after which total RNA was reverse-transcribed with M-MLV Reverse Transcriptase (Sigma). The qRT–PCR was performed with a SYBR Green kit (Sigma) on a 7500 Fast RT–PCR System (Applied Biosystems). Primer sequences are listed in Appendix Table S1. mRNA expression of genes of interest was normalized to mRNA expression of the housekeeping genes *L19*, *β-Actin*, and/or *β2-microglobulin*.

Protein isolation and Western blot analysis

Cells were stimulated with TUG-891 (10 μM) for 5 min to assess phosphorylation of ERK and AKT after which they were lysed in ice-cold RIPA buffer (50 mM Tris–HCL pH 8, 1 mM EDTA, 150 mM NaCl, 1% NP-40, 0.5% sodium deoxycholate, 0.1% SDS) containing protease and phosphatase inhibitor cocktails (Roche). Homogenates were centrifuged, and protein content of the supernatant was determined using a Coomassie Protein Assay Kit (Thermo Fisher). After heating the samples (5 min, 95°C), 20 μg of protein was separated by 12% SDS–PAGE, followed by transfer to a PVDF membrane using the Trans-Blot Turbo Transfer System (Bio-Rad). Membranes were blocked with 5% milk, incubated overnight at 4°C with protein-specific primary antibody followed by incubation for 1 h with horseradish peroxidase (HRP)-conjugated secondary antibodies (Goat anti-Rabbit HRP, Dako P0448 at 1:2,000 or Promega W4018 at 1:1,000). Primary antibodies used were rabbit anti-pHSL563 (Cell Signaling #4139 at 1:1,000), rabbit anti-UCP1 (Sigma U6382 at 1:4,000), rabbit anti-tubulin (Cell Signaling #2148 at 1:1,000), rabbit anti-pPKA substrate (Cell Signalling #9612 at 1:1,000), rabbit anti-pERK 1/2 (Cell Signaling #9101 at 1:500), rabbit anti-ERK 1/2 (Cell Signaling #4695 at 1:5,000), rabbit anti-pAKT (Ser 473) (Cell Signaling #9271 at 1:1,000), rabbit anti-AKT (Cell Signaling #9272 at 1:1,000), and mouse anti-β-Actin HRP (Santa Cruz sc-47778 at 1:5,000). Bands were visualized using Amersham ECL Prime Western Blotting Detection Reagent (GE Healthcare) and quantified using ImageJ software (Version 1.50).

Clearance of radiolabeled lipoprotein-like emulsion particles and glucose

Glycerol tri[^{3}H]oleate ([^{3}H]TO)-labeled lipoprotein-like TG-rich emulsion particles (80 nm) were prepared and characterized as described previously (Rensen *et al*, 1995), and [^{14}C]deoxyglucose ([^{14}C]DG) was added (ratio ^{3}H:^{14}C = 4:1). Mice were fasted for 6 h and injected with 200 μl of emulsion particles (1 mg TG per mouse) via the tail vein, 1 h after onset of the dark phase (i.e., 3 h after injection of TUG891 or vehicle). After 15 min, mice were sacrificed by cervical dislocation and perfused with ice-cold PBS through the heart. Thereafter, organs were harvested and weighed, and dissolved overnight at 56°C in Tissue Solubilizer (Amersham Biosciences). The uptake of [^{3}H]TO- and [^{14}C]DG-derived radioactivity was quantified and expressed per gram of wet tissue weight or per organ for organs that could be taken out quantitatively.

Microarray experiments

iBAT from GPR120 KO mice (Godinot *et al*, 2013) and WT littermates with similar body weights were analyzed. Global mRNA expression was measured using Illumina bead chip. Whole-genome expression was profiled using MouseWG-6 v2.0 Expression BeadChips (Kuhn *et al*, 2004). The summary-level data were processed using the R packages lumi 2.10.0, lumiMouseAll.db 1.18.0, and lumiMouseIDMapping 1.10.0 using nuID annotations (Du *et al*, 2007). The data were normalized using quantile normalization. Differentially expressed genes (DEGs) between WT and KO samples were detected based on a moderated *t*-test using limma on the normalized data, removing unexpressed genes. The normalized expression data were filtered using the absolute value of logFC < 0.5 and adjusted *P*-value < 0.05, converted into z-scores, and heatmap.2 was used to visualize the data. DEGs with $P < 0.05$ were submitted to DAVID (Database for Annotation, Visualization and Integrated Discovery) for functional classification by using RefSeq mRNA accession numbers. Functional clusters were considered significant for FDR (false discovery rate) < 0.01 (da Huang *et al*, 2009).

Cell culture

Previously described immortalized cell lines of primary cultures of BAT and sWAT were used for experiments (Rosell *et al*, 2014). Immortalized GPR120 KO brown adipocytes were generated in the same way as these primary culture cell lines, *that is,* by retroviral-mediated transformation of SV40 large T-antigen. Brown and white preadipocytes were cultured in DMEM/F12 (Sigma) supplemented with 10% fetal bovine serum (FBS) and penicillin–streptomycin (Sigma). Preadipocytes were differentiated with induction medium for 2 days and with maintenance medium for 6 days. The constituents of this medium and their concentrations are listed in Appendix Table S2. To assess effects of browning of white adipocytes on gene expression, the induction medium was modulated to contain 5 μM rosiglitazone, after which the cells received 1 μM of rosiglitazone during the first 4 days of maintenance. Adipocytes were used for experiments on day 7–9 of differentiation.

Oil Red O staining

Differentiated immortalized brown adipocytes were fixed with 4% paraformaldehyde (15 min, RT) and rinsed with 60% isopropanol. Cells were stained with 0.15% Oil Red O (Sigma) in 60% isopropanol (30 min, RT), after which they were washed with 60% isopropanol. Images were taken with a phase-contrast microscope (Leica).

Cellular oxygen consumption measurements

Seahorse Bioscience XF24 extracellular flux analyzer (Seahorse Bioscience) was used to measure the OCR in differentiated brown adipocytes. On day 7 of differentiation, cells were trypsinized and seeded in a 24-well Seahorse Bioscience assay plate. The next day, cells were pretreated with BAPTA-AM (25 μM; Thermo Fisher), U0126 (10 μM; Promega), or AKT 1/2 kinase inhibitor (10 μM; A6730, Sigma) for 30 min (37°C, without CO_2) before starting Seahorse analysis. Vehicle (DMSO), TUG-891, and/or CL316243 (CL) were preloaded in the reagent delivery chambers and pneumatically injected into the wells after three baseline measurements (to a final concentration of 10 μM TUG-891 or CL). Cellular O_2 consumption was measured in real time every 7 min.

Isolation of mitochondria

Brown fat mitochondria were prepared as previously described (Cannon & Nedergaard, 2008; Shabalina *et al*, 2010). Routinely, on each experimental day, three mice were anaesthetized for 1–2 min by a mixture of 79% CO_2 and 21% O_2, and decapitated. The interscapular, axillary, and cervical BAT depots were dissected out, cleaned from WAT, and pooled in ice-cold isolation buffer, SHE consisting of 250 mM sucrose, 10 mM HEPES (pH 7.2), 0.1 mM EGTA, and 2% (w/v) FA-free BSA (10775835001 Roche Diagnostics GmbH). Throughout the isolation process, the tissue was kept at 0–4°C. Tissue was minced with scissors, homogenized in SHE buffer with a motorized Potter-Elvehjem Teflon pestle, filtered through cotton gauze, and centrifuged at 8,800 *g* for 10 min. The supernatant with the floating fat layer was discarded. The resuspended homogenate was centrifuged at 800 *g* for 10 min, and the resulting supernatant was centrifuged at 8,800 *g* for 10 min. The resulting mitochondrial pellet was resuspended in 100 mM KCl, 20 mM K^+-Tes (pH 7.2), and centrifuged again at 8,800 *g* for 10 min. The final mitochondrial pellets were resuspended by hand homogenization in a small glass homogenizer in the same medium to yield a concentration of roughly 25–35 mg/ml mitochondrial protein. The concentration of mitochondrial protein was measured using fluorescamine (Fluram, 47614 Sigma-Aldrich; Udenfriend *et al*, 1972) with BSA as a standard. Mitochondria were stored on ice, and aliquots were removed as required during functional analyses.

Mitochondrial oxygen consumption measurements

For oxygen consumption measurements, isolated brown fat mitochondria (0.25 mg protein) were added to 2.0 ml of a continuously stirred incubation medium consisting of 100 mM KCl, 20 mM K^+-Tes (pH 7.2), 2 mM $MgCl_2$, 1 mM EDTA, 4 mM KPi, 3 mM malate, 5 mM pyruvate (Sigma-Aldrich), and 0.1% FA-free BSA. Oxygen consumption rates were monitored using an O2k-MultiSensor System (Oroboros Instruments) in a sealed incubation chamber at 37°C. During prolonged recording, re-oxygenation of respiratory buffer was performed by unsealing of chamber. Basal respiration was measured in the presence of 1–3 mM GDP (dissolved in 20 mM Tes (final pH 7.2), G7127 Sigma-Aldrich). Maximal oxygen consumption rates (respiratory capacity) were obtained by addition of the ionophoric uncoupling agent FCCP (C2920, Sigma-Aldrich) at a final concentration of 1.0–1.4 μM. TUG-891 was dissolved in DMSO at a stock concentration of 100 mM or 20 mM and used for titration by adding 1–2 μl to 2-ml chamber.

Calcium mobilization assays

Differentiated cells were incubated for 1 h at RT with the calcium-sensitive dye Fluo-4-AM (Invitrogen) in Krebs–Ringer bicarbonate buffer (Sigma). Hereafter, the cells were washed twice with buffer, followed by live cell imaging with a confocal laser scanning microscope (LSM 510, Zeiss) and stimulation with TUG-891 (10 μM), with or without preincubation with the GPR120 antagonist AH7614 for 5 min (100 μM; Tocris) or the Gαq inhibitor YM-254890 for 30 min (0.1 μM, Alpha Laboratories).

MitoTracker experiments

Differentiated adipocytes were incubated for 30 min with MitoTracker Green FM (125 nM; Thermo Fisher) and MitoTracker Red CMXRos (250 nM; Thermo Fisher) in DMEM/F12 (Sigma) without FBS. Hereafter, the medium was changed and live cells were imaged using a confocal LSM (Leica TCS SP8, Leica Microsystems). Adipocytes were stimulated with TUG-891 (10 μM), followed by live cell imaging for 10 min to monitor mitochondrial morphology. Control cells were monitored to correct for potential photobleaching, and corrected total cell fluorescence (CTSF, integrated density − (area of selected cell × mean fluorescence of background)) of 8–9 cells per condition was quantified using ImageJ.

cAMP measurements

Measurement of whole cell cAMP was carried out with the cAMP dynamic 2 kit (Cisbio Bioassays, 62AM4PEC) as per manufacturer's instructions. Cells were pretreated with phosphodiesterase inhibitor 3-isobutyl-1-methylxanthine (IBMX, 0.5 mM, 5 min) prior to ligand treatment and lysed in 0.1 M HCl/0.1% Triton X-100. All cAMP concentrations were corrected for protein levels.

Statistical analysis

All data are expressed as mean ± SEM. Statistical analysis was performed using two-tailed unpaired Student's *t*-test or ANOVA with Tukey's *post hoc* test using SPSS Statistics (Version 23.0). Differences between groups were considered statistically significant at $P < 0.05$.

Data availability

The microarray data from this publication have been deposited to NCBI's Gene Expression Omnibus (Edgar *et al*, 2002) and assigned

The paper explained

Problem
Activation of brown adipose tissue (BAT) could be a promising strategy to promote energy expenditure and combat obesity and related disorders. A potential target to activate BAT is G protein-coupled receptor 120 (GPR120), which is highly expressed in BAT and associated with obesity in humans. However, the therapeutic potential of GPR120 agonism and GPR120-mediated signaling in BAT remain to be elucidated.

Results
Here, we show that activation of GPR120 by the selective agonist TUG-891 acutely increased fat oxidation and reduced body weight and fat mass in mice. These effects coincided with decreased brown adipocyte lipid content and increased nutrient uptake by BAT, demonstrating that increased BAT activity could underly the improved metabolism of these mice. Mechanistically, TUG-891 activated brown adipocytes *in vitro* through GPR120-dependent and GPR120-independent mechanisms. TUG-891 stimulated the Gαq-coupled GPR120, resulting in intracellular calcium release, mitochondrial depolarization, and mitochondrial fission. In addition, TUG-891 activated mitochondrial UCP1. These mechanisms could have acted synergistically *in vivo* to stimulate mitochondrial respiration in BAT and increase energy expenditure.

Impact
Since impaired GPR120 signaling predisposes to obesity in humans, obese individuals could benefit from GPR120 activation. Indeed, our data suggest that GPR120 agonism is a promising strategy to increase lipid combustion and reduces obesity.

the GEO Series accession number GSE97145 (http://www.ncbi.nlm.nih.gov/geo/query/acc.cgi?acc=GSE97145).

Expanded View for this article is available online.

Acknowledgements
This work was supported by the Biotechnology and Biological Sciences Research Council (BB/H020233/1 & BB/P008879/1), the EU FP7 project DIABAT (HEALTH-F2-2011-278373), the Genesis Research Trust, the Danish Council for Strategic Research (11-116196), and by personal grants from the Board of Directors of Leiden University Medical Center, the Dutch Heart Foundation, and the Leiden University Fund to M.S. In addition, this work was supported by Eli Lilly and Company through the Lilly Research Award Program, the Netherlands Cardiovascular Research Initiative: an initiative with support of the Dutch Heart Foundation (CVON2011-9 GENIUS to P.C.N.R.), and the Rembrandt Institute of Cardiovascular Science (RICS to P.C.N.R.). P.C.N.R. is an Established Investigator of the Dutch Heart Foundation (2009T038). We thank Karsten Kristiansen and Tao Ma (Laboratory of Genomics and Molecular Biomedicine, Dept. of Biology, Faculty of Science, University of Copenhagen, Denmark) for assistance in generation of the GPR120 KO brown adipocyte cell line, and Claire A Mitchell (Computing and Advanced Microscopy Development Unit, Warwick Medical School, University of Warwick, Coventry, UK) for assistance with confocal imaging. We thank Barbara Cannon and Jan Nedergaard (Dept. of Molecular Biosciences, The Wenner-Gren Institute, Stockholm University, Stockholm, Sweden) for their input regarding data on mitochondrial respiration and UCP1 activation. We thank Lianne van der Wee-Pals, Trea Streefland, and Chris van der Bent (Div. of Endocrinology, Dept. of Medicine, LUMC, Leiden, The Netherlands) for their excellent technical assistance.

Author contributions
MS performed experiments, analyzed data, and drafted the manuscript. ADvD, GH, IGS, AO, ACH, LHD, IMM, NC, and SK performed experiments, and Y-WC performed bioinformatic analysis. SD provided GPR120 KO BAT used for microarray analysis. ARM and TC provided GPR120 KO mice used for experiments with TUG-891. BS synthesized TUG-891. TU provided tool compounds and contributed to the design of the study. ADvD, PCNR, and MC helped to conceptualize the project and supervised the project. All authors critically reviewed the manuscript.

Conflict of interest
The authors declare that they have no conflict of interest.

References

Argyropoulos G, Harper ME (2002) Uncoupling proteins and thermoregulation. *J Appl Physiol* 92: 2187 – 2198

Auguste S, Fisette A, Fernandes MF, Hryhorczuk C, Poitout V, Alquier T, Fulton S (2016) Central agonism of GPR120 acutely inhibits food intake and food reward and chronically suppresses anxiety-like behavior in mice. *Int J Neuropsychopharmacol* 19: pyw014

Azevedo CM, Watterson KR, Wargent ET, Hansen SV, Hudson BD, Kepczynska MA, Dunlop J, Shimpukade B, Christiansen E, Milligan G *et al* (2016) Non-acidic free fatty acid receptor 4 agonists with antidiabetic activity. *J Med Chem* 59: 8868 – 8878

Berbee JF, Boon MR, Khedoe PP, Bartelt A, Schlein C, Worthmann A, Kooijman S, Hoeke G, Mol IM, John C *et al* (2015) Brown fat activation reduces hypercholesterolaemia and protects from atherosclerosis development. *Nat Commun* 6: 6356

Blondin DP, Labbe SM, Tingelstad HC, Noll C, Kunach M, Phoenix S, Guerin B, Turcotte EE, Carpentier AC, Richard D *et al* (2014) Increased brown adipose tissue oxidative capacity in cold-acclimated humans. *J Clin Endocrinol Metab* 99: E438 – E446

Briscoe CP, Peat AJ, McKeown SC, Corbett DF, Goetz AS, Littleton TR, McCoy DC, Kenakin TP, Andrews JL, Ammala C *et al* (2006) Pharmacological regulation of insulin secretion in MIN6 cells through the fatty acid receptor GPR40: identification of agonist and antagonist small molecules. *Br J Pharmacol* 148: 619 – 628

Cannon B, Nedergaard J (2004) Brown adipose tissue: function and physiological significance. *Physiol Rev* 84: 277 – 359

Cannon B, Nedergaard J (2008) Studies of thermogenesis and mitochondrial function in adipose tissues. *Methods Mol Biol* 456: 109 – 121

Christiansen E, Watterson KR, Stocker CJ, Sokol E, Jenkins L, Simon K, Grundmann M, Petersen RK, Wargent ET, Hudson BD *et al* (2015) Activity of dietary fatty acids on FFA1 and FFA4 and characterisation of pinolenic acid as a dual FFA1/FFA4 agonist with potential effect against metabolic diseases. *Br J Nutr* 113: 1677 – 1688

Cypess AM, Lehman S, Williams G, Tal I, Rodman D, Goldfine AB, Kuo FC, Palmer EL, Tseng YH, Doria A *et al* (2009) Identification and importance of brown adipose tissue in adult humans. *N Engl J Med* 360: 1509 – 1517

Dennis G, Sherman BT, Hosack DA, Yang J, Gao W, Lane HC, Lempicki RA (2003) DAVID: database for annotation, visualization, and integrated discovery. *Genome Biol* 4: R60

Dragano NRV, Solon C, Ramalho AF, de Moura RF, Razolli DS, Christiansen E, Azevedo C, Ulven T, Velloso LA (2017) Polyunsaturated fatty acid receptors, GPR40 and GPR120, are expressed in the hypothalamus and control energy homeostasis and inflammation. *J Neuroinflammation* 14: 91

Du P, Kibbe WA, Lin SM (2007) nuID: a universal naming scheme of oligonucleotides for illumina, affymetrix, and other microarrays. *Biol Direct* 2: 16

Dunn TN, Akiyama T, Lee HW, Kim JB, Knotts TA, Smith SR, Sears DD, Carstens E, Adams SH (2015) Evaluation of the synuclein-gamma (SNCG) gene as a PPARgamma target in murine adipocytes, dorsal root ganglia somatosensory neurons, and human adipose tissue. *PLoS One* 10: e0115830

Edgar R, Domrachev M, Lash AE (2002) Gene Expression Omnibus: NCBI gene expression and hybridization array data repository. *Nucleic Acids Res* 30: 207 – 210

El-Azzouny M, Evans CR, Treutelaar MK, Kennedy RT, Burant CF (2014) Increased glucose metabolism and glycerolipid formation by fatty acids and GPR40 receptor signaling underlies the fatty acid potentiation of insulin secretion. *J Biol Chem* 289: 13575 – 13588

Enerback S, Jacobsson A, Simpson EM, Guerra C, Yamashita H, Harper ME, Kozak LP (1997) Mice lacking mitochondrial uncoupling protein are cold-sensitive but not obese. *Nature* 387: 90 – 94

Fedorenko A, Lishko PV, Kirichok Y (2012) Mechanism of fatty-acid-dependent UCP1 uncoupling in brown fat mitochondria. *Cell* 151: 400 – 413

Godinot N, Yasumatsu K, Barcos ME, Pineau N, Ledda M, Viton F, Ninomiya Y, le Coutre J, Damak S (2013) Activation of tongue-expressed GPR40 and GPR120 by non caloric agonists is not sufficient to drive preference in mice. *Neuroscience* 250: 20 – 30

Gorski JN, Pachanski MJ, Mane J, Plummer CW, Souza S, Thomas-Fowlkes BS, Ogawa AM, Weinglass AB, Di Salvo J, Cheewatrakoolpong B *et al* (2017) GPR40 reduces food intake and body weight through GLP-1. *Am J Physiol Endocrinol Metab* 313: E37 – E47

Gotoh C, Hong YH, Iga T, Hishikawa D, Suzuki Y, Song SH, Choi KC, Adachi T, Hirasawa A, Tsujimoto G *et al* (2007) The regulation of adipogenesis through GPR120. *Biochem Biophys Res Commun* 354: 591 – 597

Hirasawa A, Tsumaya K, Awaji T, Katsuma S, Adachi T, Yamada M, Sugimoto Y, Miyazaki S, Tsujimoto G (2005) Free fatty acids regulate gut incretin glucagon-like peptide-1 secretion through GPR120. *Nat Med* 11: 90 – 94

Hou Y, Kitaguchi T, Kriszt R, Tseng YH, Raghunath M, Suzuki M (2017) Ca^{2+}-associated triphasic pH changes in mitochondria during brown adipocyte activation. *Mol Metab* 6: 797 – 808

da Huang W, Sherman BT, Lempicki RA (2009) Bioinformatics enrichment tools: paths toward the comprehensive functional analysis of large gene lists. *Nucleic Acids Res* 37: 1 – 13

Hudson BD, Shimpukade B, Mackenzie AE, Butcher AJ, Pediani JD, Christiansen E, Heathcote H, Tobin AB, Ulven T, Milligan G (2013) The pharmacology of TUG-891, a potent and selective agonist of the free fatty acid receptor 4 (FFA4/GPR120), demonstrates both potential opportunity and possible challenges to therapeutic agonism. *Mol Pharmacol* 84: 710 – 725

Ichimura A, Hirasawa A, Poulain-Godefroy O, Bonnefond A, Hara T, Yengo L, Kimura I, Leloire A, Liu N, Iida K *et al* (2012) Dysfunction of lipid sensor GPR120 leads to obesity in both mouse and human. *Nature* 483: 350 – 354

Itoh Y, Kawamata Y, Harada M, Kobayashi M, Fujii R, Fukusumi S, Ogi K, Hosoya M, Tanaka Y, Uejima H *et al* (2003) Free fatty acids regulate insulin secretion from pancreatic beta cells through GPR40. *Nature* 422: 173 – 176

Kebede M, Alquier T, Latour MG, Semache M, Tremblay C, Poitout V (2008) The fatty acid receptor GPR40 plays a role in insulin secretion *in vivo* after high-fat feeding. *Diabetes* 57: 2432 – 2437

Kim N, Lee JO, Lee HJ, Kim HI, Kim JK, Lee YW, Lee SK, Kim SJ, Park SH, Kim HS (2015) Endogenous ligand for GPR120, docosahexaenoic acid, exerts benign metabolic effects on the skeletal muscles via AMP-activated protein kinase pathway. *J Biol Chem* 290: 20438 – 20447

Kuhn K, Baker SC, Chudin E, Lieu MH, Oeser S, Bennett H, Rigault P, Barker D, McDaniel TK, Chee MS (2004) A novel, high-performance random array platform for quantitative gene expression profiling. *Genome Res* 14: 2347 – 2356

van der Lans AA, Hoeks J, Brans B, Vijgen GH, Visser MG, Vosselman MJ, Hansen J, Jorgensen JA, Wu J, Mottaghy FM *et al* (2013) Cold acclimation recruits human brown fat and increases nonshivering thermogenesis. *J Clin Invest* 123: 3395 – 3403

Liu D, Wang L, Meng Q, Kuang H, Liu X (2012) G-protein coupled receptor 120 is involved in glucose metabolism in fat cells. *Cell Mol Biol* 58: 1757 – 1762

Mandard S, Stienstra R, Escher P, Tan NS, Kim I, Gonzalez FJ, Wahli W, Desvergne B, Muller M, Kersten S (2007) Glycogen synthase 2 is a novel target gene of peroxisome proliferator-activated receptors. *Cell Mol Life Sci* 64: 1145 – 1157

van Marken Lichtenbelt WD, Vanhommerig JW, Smulders NM, Drossaerts JM, Kemerink GJ, Bouvy ND, Schrauwen P, Teule GJ (2009) Cold-activated brown adipose tissue in healthy men. *N Engl J Med* 360: 1500 – 1508

Matthias A, Ohlson KB, Fredriksson JM, Jacobsson A, Nedergaard J, Cannon B (2000) Thermogenic responses in brown fat cells are fully UCP1-dependent. UCP2 or UCP3 do not substitute for UCP1 in adrenergically or fatty acid-induced thermogenesis. *J Biol Chem* 275: 25073 – 25081

Nicholls DG (2017) The hunt for the molecular mechanism of brown fat thermogenesis. *Biochimie* 134: 9 – 18

Oh DY, Talukdar S, Bae EJ, Imamura T, Morinaga H, Fan W, Li P, Lu WJ, Watkins SM, Olefsky JM (2010) GPR120 is an omega-3 fatty acid receptor mediating potent anti-inflammatory and insulin-sensitizing effects. *Cell* 142: 687 – 698

Ohno H, Shinoda K, Spiegelman BM, Kajimura S (2012) PPARgamma agonists induce a white-to-brown fat conversion through stabilization of PRDM16 protein. *Cell Metab* 15: 395 – 404

Ou HY, Wu HT, Hung HC, Yang YC, Wu JS, Chang CJ (2013) Multiple mechanisms of GW-9508, a selective G protein-coupled receptor 40 agonist, in the regulation of glucose homeostasis and insulin sensitivity. *Am J Physiol Endocrinol Metab* 304: E668 – E676

Pajouhesh H, Lenz GR (2005) Medicinal chemical properties of successful central nervous system drugs. *NeuroRx* 2: 541 – 553

Pendergrass W, Wolf N, Poot M (2004) Efficacy of MitoTracker Green and CMXrosamine to measure changes in mitochondrial membrane potentials in living cells and tissues. *Cytometry A* 61: 162 – 169

Peronnet F, Massicotte D (1991) Table of nonprotein respiratory quotient: an update. *Can J Sport Sci* 16: 23 – 29

Quesada-López T, Cereijo R, Turatsinze JV, Planavila A, Cairó M, Gavaldà-Navarro A, Peyrou M, Moure R, Iglesias R, Giralt M *et al* (2016) The lipid sensor GPR120 promotes brown fat activation and FGF21 release from adipocytes. *Nat Commun* 7: 13479

Rensen PC, van Dijk MC, Havenaar EC, Bijsterbosch MK, Kruijt JK, van Berkel TJ (1995) Selective liver targeting of antivirals by recombinant chylomicrons–a new therapeutic approach to hepatitis B. *Nat Med* 1: 221 – 225

Rosell M, Kaforou M, Frontini A, Okolo A, Chan YW, Nikolopoulou E, Millership S, Fenech ME, Macintyre D, Turner JO *et al* (2014) Brown and white adipose tissues: intrinsic differences in gene expression and

response to cold exposure in mice. *Am J Physiol Endocrinol Metab* 306: E945 – E964

Schilperoort M, Hoeke G, Kooijman S, Rensen PC (2016) Relevance of lipid metabolism for brown fat visualization and quantification. *Curr Opin Lipidol* 27: 242 – 248

Shabalina IG, Jacobsson A, Cannon B, Nedergaard J (2004) Native UCP1 displays simple competitive kinetics between the regulators purine nucleotides and fatty acids. *J Biol Chem* 279: 38236 – 38248

Shabalina IG, Ost M, Petrovic N, Vrbacky M, Nedergaard J, Cannon B (2010) Uncoupling protein-1 is not leaky. *Biochim Biophys Acta* 1797: 773 – 784

Shimpukade B, Hudson BD, Hovgaard CK, Milligan G, Ulven T (2012) Discovery of a potent and selective GPR120 agonist. *J Med Chem* 55: 4511 – 4515

Trayhurn P (2017) Origins and early development of the concept that brown adipose tissue thermogenesis is linked to energy balance and obesity. *Biochimie* 134: 62 – 70

Udenfriend S, Stein S, Bohlen P, Dairman W, Leimgruber W, Weigele M (1972) Fluorescamine: a reagent for assay of amino acids, peptides, proteins, and primary amines in the picomole range. *Science* 178: 871 – 872

Virtanen KA, Lidell ME, Orava J, Heglind M, Westergren R, Niemi T, Taittonen M, Laine J, Savisto NJ, Enerback S *et al* (2009) Functional brown adipose tissue in healthy adults. *N Engl J Med* 360: 1518 – 1525

Wikstrom JD, Mahdaviani K, Liesa M, Sereda SB, Si Y, Las G, Twig G, Petrovic N, Zingaretti C, Graham A *et al* (2014) Hormone-induced mitochondrial fission is utilized by brown adipocytes as an amplification pathway for energy expenditure. *EMBO J* 33: 418 – 436

Witte N, Muenzner M, Rietscher J, Knauer M, Heidenreich S, Nuotio-Antar AM, Graef FA, Fedders R, Tolkachov A, Goehring I *et al* (2015) The glucose sensor ChREBP links *de novo* lipogenesis to PPARgamma activity and adipocyte differentiation. *Endocrinology* 156: 4008 – 4019

Yoneshiro T, Aita S, Matsushita M, Kayahara T, Kameya T, Kawai Y, Iwanaga T, Saito M (2013) Recruited brown adipose tissue as an antiobesity agent in humans. *J Clin Invest* 123: 3404 – 3408

The GPR120 agonist TUG-891 promotes metabolic health by stimulating mitochondrial respiration in brown fat

Appendix

Table of contents:

Appendix Table S1. Primer sequences for qRT-PCR.

Gene	Primer sequence		Product length (bp)
Aacs	Forward	5'- CTGTCAGTGCTGGAGGAGAA -3'	191
	Reverse	5'- TGGCCCATGAAACAGGAGAT -3'	
Acaa2	Forward	5'- AGAAGGCCCTGGATCTTGAC -3'	162
	Reverse	5'- CTCCAATGCAAGCTGATCCC -3'	
Acc1	Forward	5'- TGTCCACCCAAGCATTTCTTC -3'	75
	Reverse	5'- CATCCAACACCAGTTCAGTATACGT -3'	
Acc2	Forward	5'- ACTTTGACCTGACCGCTGTG -3'	129
	Reverse	5'- CTGAGTGCCGGATAATGGC -3'	
Acsl1	Forward	5'- CAGAACCCGAAGATCTTGCG -3'	192
	Reverse	5'- CGGTCTCAAACATATGGGCG -3'	
Adcy4	Forward	5'- CCTCATTGCCCGCCTTTATC -3'	195
	Reverse	5'- GTCTCAGTCTCCTCTCGCTC -3'	
Adhfe1	Forward	5'- CCAGCTCCCTCCTGTACAAA -3'	159
	Reverse	5'- CCCACAGCAACATAGGCATC -3'	
Adrb3	Forward	5'- ATCGTGTCCGCTGCCGT -3'	63
	Reverse	5'- ATCTGCCCCTACACGCCAC -3'	
Aldh2	Forward	5'- GAGCAGAGCCATGTCATGTG -3'	218
	Reverse	5'- TGTCACACATCCAGGCATCT -3'	
aP2	Forward	5'- ACACCGAGATTTCCTTCAAACTG -3'	88
	Reverse	5'- CCATCTAGGGTTATGATGCTCTTCA -3'	
Apoc1	Forward	5'- GAGGGCGGTGGTGAATACTA -3'	183
	Reverse	5'- ATGCTCTCCAATGTTCCGGA -3'	
Atgl	Forward	5'- GCCAATGTCTGCAGCACATT -3'	73
	Reverse	5'- CATAGCGCACCCCTTGGA -3'	
Ccl2 (Mcp1)	Forward	5'- CAGGTCCCTGTCATGCTTCT -3'	93
	Reverse	5'- GAGTGGGGCGTTAACTGCAT -3'	
Ccl5 (Rantes)	Forward	5'- GCAAGTGCTCCAATCTTGCA -3'	71
	Reverse	5'- CTTCTCTGGGTTGGCACACA -3'	
Ccna	Forward	5'- CTGAAGGCCGGGAACGTG -3'	73
	Reverse	5'- CCTTAAGAGGAGCAACCCGT -3'	
Ccnb	Forward	5'- AAATTGCAGCTGGGGCTTTC -3'	70
	Reverse	5'- TGCAGAGTTGGTGTCCATTCA -3'	
Cd36	Forward	5'- GATGTGGAACCCATAACTGGA -3'	71
	Reverse	5'- GGCTTGACCAATATGTTGACC -3'	
Cd68	Forward	5'- CCAATTCAGGGTGGAAGAAA -3'	104
	Reverse	5'- GAGAGAGACAGGTGGGGATG -3'	
Cidea	Forward	5'- CACGCATTTCATGATCTTGGA -3'	74
	Reverse	5'- GTTGCTTGCAGACTGGGACAT -3'	
Ctgf	Forward	5'- AGCTGGGAGAACTGTGTACG -3'	380
	Reverse	5'- GCCAAATGTGTCTTCCAGTC -3'	
Dgat2	Forward	5'- TCGCGAGTACCTGATGTCTG -3'	160
	Reverse	5'- CTTCAGGGTGACTGCGTTCT -3'	
Fasn	Forward	5'- TGCGGAAACTTCAGGAAATGT -3'	82
	Reverse	5'- AGAGACGTGTCACTCCTGGACTT -3'	
Gadd45a	Forward	5'- GCTGCCAAGCTGCTCAAC -3'	71
	Reverse	5'- TCGTCGTCTTCGTCAGCA -3'	
G0s2	Forward	5'- AGTGCTGCCTCTCTTCCCAC -3'	65
	Reverse	5'- TTTCCATCTGAGCTCTGGGC -3'	
Glut1	Forward	5'- GACGGGCCGCCTCATGTTGG -3'	140
	Reverse	5'- GCTCTCCGTAGCGGTGGTTCC -3'	

Glut4	Forward Reverse	5'- CTATTCAACCAGCATCTTCGAG -3' 5'- CTACTAAGAGCACCGAGACC -3'	110
Gpr120	Forward Reverse	5'- CCCCTCTGCATCTTGTTCC -3' 5'- GATTTCTCCTATGCGGTTGG -3'	102
Gys2	Forward Reverse	5'- ATCCTTTCTCGTGCCAGGAA -3' 5'- GCGGTGGTATATCTGCCTCT -3'	159
Hsl	Forward Reverse	5'- CGAGACAGGCCTCAGTGTGA -3' 5'- TCTGGGTCTATGGCGAATCG -3'	66
Il6	Forward Reverse	5'- CTCTGGGAAATCGTGGAAAT -3' 5'- CCAGTTTGGTAGCATCCATC -3'	134
Insr	Forward Reverse	5'- CTACAGTGTTCGAGTCCGGG -3' 5'- TGGCAATATTTGATGGGACATCT -3'	107
L19	Forward Reverse	5'- GGAAAAAGAAGGTCTGGTTGGA -3' 5'- TGATCTGCTGACGGGAGTTG -3'	72
Lgals3	Forward Reverse	5'- CAACCATCGGATGAAGAACC -3' 5'- TTCCCACTCCTAAGGCACAC -3'	141
Lpl	Forward Reverse	5'- CAAGACCTTCGTGGTGATCCA -3' 5'- GTACAGGGCGGCCACAAGT -3'	82
Mki67	Forward Reverse	5'- ACAGGCTCCGTACTTTCCAA -3' 5'- ACTGGATAGCACTTTTTCTCCCAA -3'	120
Mlxipl	Forward Reverse	5'- CCCTCAGACACCCACATCTT -3' 5'- TCAGAAAGGGGTTGGGATCC -3'	209
Murf1	Forward Reverse	5'- TGTGCAAGGAACACGAAGAC -3' 5'- CCAGCATGGAGATGCAGTTA -3'	171
Myog	Forward Reverse	5'- CCCAACCCAGGAGATCATTT -3' 5'- GTCTGGGAAGGCAACAGACA -3'	117
Paqr9	Forward Reverse	5'- GGTTTGCGTGGAGTTTCTGT -3' 5'- TGTTTCACCTCCCATCTCCC -3'	172
Pgc1α	Forward Reverse	5'- GATGGCACGCAGCCCTAT -3' 5'- CTCGACACGGAGAGTTAAAGGAA -3'	70
Pnpla3	Forward Reverse	5'- ACCTGAGAGCCTGCAATCTT -3' 5'- AACAGAACCCTTCCCAGAGG -3'	217
Pgc1α	Forward Reverse	5'- GATGGCACGCAGCCCTAT -3' 5'- CTCGACACGGAGAGTTAAAGGAA -3'	70
Pparα	Forward Reverse	5'- ATGCCAGTACTGCCGTTTTC -3' 5'- GGCCTTGACCTTGTTCATGT -3'	220
Pparγ	Forward Reverse	5'- TTGTAGAGTGCCAGGTGCTG -3' 5'- CCTCCATAGCTCAGGTGGAA -3'	151
Scd1	Forward Reverse	5'- CCCCTGCGGATCTTCCTTAT -3' 5'- AGGGTCGGCGTGTGTTTCT -3'	114
Scd2	Forward Reverse	5'- AGCGGGCTGCAGAAACTTAG -3' 5'- GGCTGAGTAAGCGCCAGAGAT -3'	148
Sncg	Forward Reverse	5'- CAAGGAAGGTGTTGTGGGTG -3' 5'- CTTGTTGGCCACTGTGTTGA -3'	208
Srebp1c	Forward Reverse	5'- ATGCCATGGGCAAGTACACA -3' 5'- ATAGCATCTCCTGCGCACTC -3'	91
Tnfα	Forward Reverse	5'- ATGAGAAGTTCCCAAATGGC -3' 5'- CTCCACTTGGTGGTTTGCTA -3'	125
Ucp1	Forward Reverse	5'- TACCCAAGCGTACCAAGCTG -3' 5'- ACCCGAGTCGCAGAAAAGAA -3'	97
Vegf	Forward Reverse	5'- CATCTTCAAGCCGTCCTGTGT -3' 5'- CTCCAGGGCTTCATCGTTACA -3'	67
Vldlr	Forward Reverse	5'- GCCCTGAACAGTGCCATATG -3' 5'- CATCACTGCCATCGTCACAG -3'	243

β-Actin	Forward Reverse	5'- GCAGGAGTACGATGAGTCCG -3' 5'- ACGCAGCTCAGTAACAGT -3'	74
β-2 microglobulin	Forward Reverse	5'- TGACCGGCTTGTATGCTATC -3' 5'- CAGTGTGAGCCAGGATATAG -3'	222

Appendix Table S2. Culture medium compounds and their concentrations.

Compound	ImBA Induction	ImBA Maintenance	ImWA Induction	ImWA Maintenance
Thyroid hormone T_3	1 nM	1 nM	0.1 nM	0.1 nM
Insulin	1 μg/ml	1 μg/ml	5 μg/ml	5 μg/ml
Biotin	16 μM	16 μM	16 μM	16 μM
Pantothenate	1.8 μM	1.8 μM	1.8 μM	1.8 μM
Ascorbic acid	100 μM	100 μM	100 μM	100 μM
IBMX	0.5 mM	-	0.5 mM	-
Dexamethasone	250 nM	-	250 nM	-
Indomethacin	125 μM	-	-	-
Cortisol	-	-	100 nM	-
Rosiglitazone	-	-	1 μM	-

ImBA: immortalized brown adipocytes, ImWA: immortalized white adipocytes.

Appendix Table S3. Genes upregulated or downregulated in the absence of GPR120.

Table S3A. Genes upregulated in BAT from GPR120 KO versus WT mice.

Gene Symbol	Gene Name	FC	Adj P Value
Sncg	synuclein, gamma	1.99	0.037
Xlr4a	X-linked lymphocyte-regulated 4A	1.86	0.047
Npm3-ps1	nucleoplasmin 3, pseudogene 1	1.75	0.039
Cd52	CD52 antigen	1.71	0.014
Rarres2	retinoic acid receptor responder (tazarotene induced) 2	1.71	0.021
Hist1h2ap	histone cluster 1, H2ap	1.68	0.011
Wdfy1	WD repeat and FYVE domain containing 1	1.67	0.021
Cxcl9	chemokine (C-X-C motif) ligand 9	1.65	0.011
Hist1h2ad	histone cluster 1, H2ad	1.62	0.011
Ccl11	chemokine (C-C motif) ligand 11	1.62	0.023
Npm3	nucleoplasmin 3	1.52	0.040
Hebp1	heme binding protein 1	1.52	0.013
Coro1a	coronin, actin binding protein 1A	1.52	0.008
Hn1	hematological and neurological expressed sequence 1	1.50	0.023
Rps12-ps24	Ribosomal protein S12, pseudogene 24	1.49	0.028
Cd74	CD74 antigen (invariant polypeptide of major histocompatibility complex, class II antigen-associated)	1.48	0.045
Hist1h2ai	histone cluster 1, H2ai	1.48	0.022
Sae1	SUMO1 activating enzyme subunit 1	1.48	0.009

Gm11425	predicted gene 11425	1.46	0.034
Psmb9	proteasome (prosome, macropain) subunit, beta type 9 (large multifunctional peptidase 2)	1.45	0.005
Slamf9	SLAM family member 9	1.45	0.031
Pigp	phosphatidylinositol glycan anchor biosynthesis, class P	1.45	0.034
Maged2	melanoma antigen, family D, 2	1.45	0.011
H2-Eb1	histocompatibility 2, class II antigen E beta	1.44	0.034
Hist1h2af	histone cluster 1, H2af	1.44	0.027
Dus4l	dihydrouridine synthase 4-like (S. cerevisiae)	1.43	0.029
Wbp5	WW domain binding protein 5	1.42	0.037
Rpl12	ribosomal protein L12	1.41	0.031
Rps5	ribosomal protein S5	1.41	0.046
1110059E24Rik	RIKEN cDNA 1110059E24 gene	1.41	0.003
Mettl20	Methyltransferase like 20	1.41	0.025
Anxa2	annexin A2	1.40	0.004
Mgst3	microsomal glutathione S-transferase 3	1.39	0.026
Nsmce1	non-SMC element 1 homolog (S. cerevisiae)	1.39	0.021
Hist1h2an	histone cluster 1, H2an	1.39	0.027
Lsm5	LSM5 homolog, U6 small nuclear RNA associated (S. cerevisiae)	1.38	0.034
Mpeg1	macrophage expressed gene 1	1.38	0.025
Ubxn6	UBX domain protein 6	1.38	0.023
Rps12	ribosomal protein S12	1.38	0.026
Evi2a	ecotropic viral integration site 2a	1.38	0.034
Arhgdib	Rho, GDP dissociation inhibitor (GDI) beta	1.38	0.036
Fbn1	fibrillin 1	1.37	0.049
Rps26	ribosomal protein S26	1.37	0.034
Rhoj	ras homolog gene family, member J	1.37	0.015
Ugt1a10	UDP glycosyltransferase 1 family, polypeptide A10	1.37	0.034
Mgst3	microsomal glutathione S-transferase 3	1.36	0.009
Tyrobp	TYRO protein tyrosine kinase binding protein	1.36	0.031
Ebpl	emopamil binding protein-like	1.36	0.016
Arpc3	actin related protein 2/3 complex, subunit 3	1.36	0.033
Siva1	SIVA1, apoptosis-inducing factor	1.35	0.040

Table S3B. Genes downregulated in BAT from GPR120 KO versus WT mice.

Gene Symbol	**Gene Name**	**FC**	**Adj P Value**
O3far1	omega-3 fatty acid receptor 1	0.35	0.002
Pnpla3	patatin-like phospholipase domain containing 3	0.38	0.016
Hspa8	heat shock protein 8	0.41	0.001
Cyp2b10	cytochrome P450, family 2, subfamily b, polypeptide 10	0.43	0.038
Adrbk2	adrenergic receptor kinase, beta 2	0.55	0.004
Vegfa	vascular endothelial growth factor A	0.55	0.003
Apoc1	apolipoprotein C-I	0.55	0.004
Mlxipl	MLX interacting protein-like	0.56	0.007
Hspd1	heat shock protein 1 (chaperonin)	0.56	0.017
Luc7l3	LUC7-like 3 (S. cerevisiae)	0.58	0.015
Per2	period homolog 2 (Drosophila)	0.60	0.011
Atl2	atlastin GTPase 2	0.60	0.034
Neat1	nuclear paraspeckle assembly transcript 1 (non-protein	0.61	0.050

	coding)		
Acsl1	acyl-CoA synthetase long-chain family member 1	0.61	0.041
Ggnbp1	gametogenetin binding protein 1	0.61	0.011
Slc4a4	solute carrier family 4 (anion exchanger), member 4	0.61	0.014
Per2	period homolog 2 (Drosophila)	0.61	0.021
Rnf44	ring finger protein 44	0.62	0.023
Flcn	folliculin	0.62	0.028
Slc25a20	solute carrier family 25 (mitochondrial carnitine/acylcarnitine translocase), member 20	0.62	0.025
Atl2	atlastin GTPase 2	0.62	0.047
Hnrpdl	heterogeneous nuclear ribonucleoprotein D-like	0.62	0.011
Srsf2	serine/arginine-rich splicing factor 2	0.63	0.016
Slc38a2	solute carrier family 38, member 2	0.63	0.016
Gys2	glycogen synthase 2	0.63	0.023
Ddx17	DEAD (Asp-Glu-Ala-Asp) box polypeptide 17	0.63	0.014
Gm3308	predicted gene 3308	0.64	0.021
Gm10621	predicted gene 10621	0.64	0.004
Ccrn4l	CCR4 carbon catabolite repression 4-like (S. cerevisiae)	0.64	0.024
Actb	actin, beta	0.64	0.021
Aspg	asparaginase homolog (S. cerevisiae)	0.64	0.021
Clasrp	CLK4-associating serine/arginine rich protein	0.64	0.013
Pparγc1b	peroxisome proliferative activated receptor, gamma, coactivator 1 beta	0.64	0.029
Apoc1	apolipoprotein C-I	0.65	0.034
Hnrnpa2b1	heterogeneous nuclear ribonucleoprotein A2/B1	0.65	0.017
Adhfe1	alcohol dehydrogenase, iron containing, 1	0.65	0.028
Klf9	Kruppel-like factor 9	0.65	0.029
Aacs	acetoacetyl-CoA synthetase	0.66	0.039
Vegfα	vascular endothelial growth factor A	0.66	0.003
Srrm2	serine/arginine repetitive matrix 2	0.66	0.013
2810403A07Rik	RIKEN cDNA 2810403A07 gene	0.67	0.011
Hsp90ab1	heat shock protein 90 alpha (cytosolic), class B member 1	0.67	0.046
Gtf3c2	general transcription factor IIIC, polypeptide 2, beta	0.67	0.011
Lgals4	lectin, galactose binding, soluble 4	0.67	0.011
Paqr9	progestin and adipoQ receptor family member IX	0.67	0.030
Arap3	ArfGAP with RhoGAP domain, ankyrin repeat and PH domain 3	0.68	0.030
Slc1a5	solute carrier family 1 (neutral amino acid transporter), member 5	0.68	0.001
Fam126b	family with sequence similarity 126, member B	0.68	0.022
Slc1a5	solute carrier family 1 (neutral amino acid transporter), member 5	0.68	0.003
Gm2589	predicted gene 2589	0.68	0.012

FC: fold change.

Appendix Table S4. Functional annotation clustering of genes upregulated or downregulated in the absence of GPR120.

Table S4A. DAVID (P=0.05), upregulated in GPR120 KO, 7 clusters with terms with FDR < 0.01.

Annotation Cluster 1	**Enrichment Score: 23.571326366746383**	
Category	**Term**	**FDR**
GOTERM_MF_FAT	GO:0003735~structural constituent of ribosome	3.18E-27
SP_PIR_KEYWORDS	ribonucleoprotein	4.17E-26
KEGG_PATHWAY	mmu03010:Ribosome	6.46E-25
GOTERM_CC_FAT	GO:0005840~ribosome	3.05E-24
SP_PIR_KEYWORDS	ribosomal protein	3.34E-24
GOTERM_CC_FAT	GO:0030529~ribonucleoprotein complex	2.50E-23
GOTERM_BP_FAT	GO:0006412~translation	2.83E-21
GOTERM_MF_FAT	GO:0005198~structural molecule activity	1.14E-10
GOTERM_CC_FAT	GO:0033279~ribosomal subunit	3.05E-08
Annotation Cluster 2	**Enrichment Score: 5.009748166504468**	
Category	**Term**	**FDR**
GOTERM_CC_FAT	GO:0043228~non-membrane-bounded organelle	5.14E-05
GOTERM_CC_FAT	GO:0043232~intracellular non-membrane-bounded organelle	5.14E-05
Annotation Cluster 3	**Enrichment Score: 3.6450159174973065**	
Category	**Term**	**FDR**
GOTERM_BP_FAT	GO:0006396~RNA processing	3.92 E-03
Annotation Cluster 6	**Enrichment Score: 3.083826976916491**	
Category	**Term**	**FDR**
GOTERM_BP_FAT	GO:0048002~antigen processing and presentation of peptide antigen	1.72E-08
GOTERM_BP_FAT	GO:0002478~antigen processing and presentation of exogenous peptide antigen	7.16E-06
GOTERM_BP_FAT	GO:0019882~antigen processing and presentation	9.29E-06
GOTERM_BP_FAT	GO:0019884~antigen processing and presentation of exogenous antigen	1.00E-05
GOTERM_BP_FAT	GO:0002495~antigen processing and presentation of peptide antigen via MHC class II	1.38E-05
GOTERM_BP_FAT	GO:0019886~antigen processing and presentation of exogenous peptide antigen via MHC class II	1.38E-05
GOTERM_BP_FAT	GO:0002504~antigen processing and presentation of peptide or polysaccharide antigen via MHC class II	1.33E-04
Annotation Cluster 15	**Enrichment Score: 2.4342394169368364**	
Category	**Term**	**FDR**
GOTERM_BP_FAT	GO:0002443~leukocyte mediated immunity	1.62E-03
GOTERM_BP_FAT	GO:0002252~immune effector process	3.34E-03
GOTERM_BP_FAT	GO:0050778~positive regulation of immune response	4.05E-03
GOTERM_BP_FAT	GO:0048584~positive regulation of response to stimulus	6.99E-03
Annotation Cluster 17	**Enrichment Score: 2.306287251432978**	

Category	Term	FDR
GOTERM_BP_FAT	GO:0050778~positive regulation of immune response	4.05E-03
Annotation Cluster 30	**Enrichment Score: 1.6629313948276978**	
Category	**Term**	**FDR**
KEGG_PATHWAY	mmu05322:Systemic lupus erythematosus	6.07E-03

Table S4B. DAVID (P=0.05), downregulated in GPR120 KO, 11 clusters with terms with FDR < 0.01.

Annotation Cluster 1	**Enrichment Score: 18.04039228677734**	
Category	**Term**	**FDR**
GOTERM_CC_FAT	GO:0005739~mitochondrion	1.54E-21
SP_PIR_KEYWORDS	mitochondrion	3.77E-18
SP_PIR_KEYWORDS	transit peptide	1.19E-15
UP_SEQ_FEATURE	transit peptide: Mitochondrion	4.19E-12
GOTERM_CC_FAT	GO:0044429~mitochondrial part	1.58E-10
Annotation Cluster 2	**Enrichment Score: 10.830871851860504**	
Category	**Term**	**FDR**
SP_PIR_KEYWORDS	mitochondrion	3.77E-18
GOTERM_CC_FAT	GO:0031090~organelle membrane	1.56E-11
GOTERM_CC_FAT	GO:0044429~mitochondrial part	1.58E-10
GOTERM_CC_FAT	GO:0031966~mitochondrial membrane	9.36E-08
GOTERM_CC_FAT	GO:0019866~organelle inner membrane	1.02E-07
GOTERM_CC_FAT	GO:0031967~organelle envelope	6.85E-07
GOTERM_CC_FAT	GO:0031975~envelope	8.04E-07
GOTERM_CC_FAT	GO:0005740~mitochondrial envelope	1.09E-06
GOTERM_CC_FAT	GO:0005743~mitochondrial inner membrane	1.34E-06
Annotation Cluster 3	**Enrichment Score: 9.454393303217916**	
Category	**Term**	**FDR**
GOTERM_MF_FAT	GO:0000166~nucleotide binding	1.68E-17
GOTERM_MF_FAT	GO:0017076~purine nucleotide binding	1.51E-08
GOTERM_MF_FAT	GO:0001882~nucleoside binding	4.75E-08
GOTERM_MF_FAT	GO:0001883~purine nucleoside binding	5.33E-08
GOTERM_MF_FAT	GO:0030554~adenyl nucleotide binding	9.68E-08
GOTERM_MF_FAT	GO:0032553~ribonucleotide binding	5.60E-06
GOTERM_MF_FAT	GO:0032555~purine ribonucleotide binding	5.60E-06
SP_PIR_KEYWORDS	nucleotide-binding	6.45E-06
SP_PIR_KEYWORDS	ATP-binding	1.09E-05
GOTERM_MF_FAT	GO:0005524~ATP binding	1.81E-05
GOTERM_MF_FAT	GO:0032559~adenyl ribonucleotide binding	3.84E-05
Annotation Cluster 4	**Enrichment Score: 8.909158524499384**	
Category	**Term**	**FDR**
GOTERM_CC_FAT	GO:0031974~membrane-enclosed lumen	7.00E-11
GOTERM_CC_FAT	GO:0070013~intracellular organelle lumen	9.83E-11
GOTERM_CC_FAT	GO:0043233~organelle lumen	1.20E-10
GOTERM_CC_FAT	GO:0031981~nuclear lumen	2.30E-05
GOTERM_CC_FAT	GO:0016607~nuclear speck	6.01E-05

GOTERM_CC_FAT	GO:0016604~nuclear body	4.99E-04
GOTERM_CC_FAT	GO:0005654~nucleoplasm	5.15E-03
Annotation Cluster 5	**Enrichment Score: 8.144022074819771**	
Category	**Term**	**FDR**
GOTERM_CC_FAT	GO:0044429~mitochondrial part	1.58E-10
GOTERM_CC_FAT	GO:0005759~mitochondrial matrix	2.59E-03
GOTERM_CC_FAT	GO:0031980~mitochondrial lumen	2.59E-03
Annotation Cluster 6	**Enrichment Score: 8.114976494819215**	
Category	**Term**	**FDR**
INTERPRO	IPR012677:Nucleotide-binding, alpha-beta plait	1.94E-09
INTERPRO	IPR000504:RNA recognition motif, RNP-1	6.55E-09
SP_PIR_KEYWORDS	RNA-binding	2.95E-08
SMART	SM00360:RRM	9.91E-08
GOTERM_MF_FAT	GO:0003723~RNA binding	1.84E-06
UP_SEQ_FEATURE	domain:RRM 1	1.36E-03
UP_SEQ_FEATURE	domain:RRM 2	1.36E-03
Annotation Cluster 7	**Enrichment Score: 5.577820081203797**	
Category	**Term**	**FDR**
GOTERM_BP_FAT	GO:0016071~mRNA metabolic process	2.99E-05
GOTERM_BP_FAT	GO:0006397~mRNA processing	6.49E-05
SP_PIR_KEYWORDS	mRNA processing	6.53E-05
GOTERM_BP_FAT	GO:0008380~RNA splicing	8.83E-05
GOTERM_BP_FAT	GO:0006396~RNA processing	3.05E-04
SP_PIR_KEYWORDS	mRNA splicing	4.12E-04
Annotation Cluster 8	**Enrichment Score: 4.573455401588822**	
Category	**Term**	**FDR**
SP_PIR_KEYWORDS	fatty acid metabolism	1.78E-03
Annotation Cluster 9	**Enrichment Score: 4.428903499912428**	
Category	**Term**	**FDR**
SP_PIR_KEYWORDS	Flavoprotein	5.53E-05
GOTERM_MF_FAT	GO:0050662~coenzyme binding	2.56E-03
SP_PIR_KEYWORDS	FAD	2.78E-03
Annotation Cluster 11	**Enrichment Score: 3.7314344007433613**	
Category	**Term**	**FDR**
GOTERM_CC_FAT	GO:0005777~peroxisome	9.14E-04
GOTERM_CC_FAT	GO:0042579~microbody	9.14E-04
Annotation Cluster 47	**Enrichment Score: 1.4911957984288633**	
Category	**Term**	**FDR**
SP_PIR_KEYWORDS	nucleus	2.20E-04

FDR: false discovery rate.

Appendix Table S5. *P*-values from statistical tests.

Figure	*P*-value		
	Vehicle versus TUG-891		
1A	1.5 wks: 0.0373 (*) 2.5 wks: 0.0047 (**)		
1B	0.75 wks: 0.0302 (*) 1.5 wks: 0.0016 (**) 2.5 wks: 0.0001(***)		
1C	2.5 wks: 0.0122 (*)		
1D	2 wks: 0.0020 (**)		
1E	Dark: 0.0045 (**)		
1F	Light: 0.0433 (*) Dark: 0.0221 (*)		
1G	Dark: 0.0040 (*)		
	Vehicle versus TUG-891		
2A	0.0075 (**)		
2B	0.0014 (**)		
2C	0.0000 (***)		
2D	iBAT: 0.0002 (***) gWAT: 0.0000 (***) Liver: 0.0093 (*)		
	Vehicle versus WT TUG-891	**Vehicle versus KO TUG-891**	**WT TUG-891 versus KO TUG-891**
3A	12 d: 0.0163 (*)	n.s.	n.s.
3B	12 d: 0.0224 (*)	n.s.	n.s.
3C	6-12 d: 0.0094 (**)	6-12 d: 0.0260 (*)	n.s.
3F	Dark: 0.0349 (*)	n.s.	n.s.
	Vehicle versus WT TUG-891	**Vehicle versus KO TUG-891**	**WT TUG-891 versus KO TUG-891**
4A	iBAT: 0.0000 (***) sBAT: 0.0000 (***)	iBAT: 0.0192 (*) sBAT: 0.0001 (***)	iBAT: 0.0000 (***) sBAT: 0.0000 (***)
4B	iBAT: 0.0290 (*) sBAT: 0.0000 (***)	n.s.	iBAT: 0.006283 (**) sBAT: 0.0000 (***)
4C	iBAT: 0.0000 (***) sWAT: 0.0149 (*)	Liver: 0.0024 (**)	n.d.
	Vehicle versus TUG-891		
5C	*Sncg*: 0.0118 (*) *Mlxipl*: 0.0368 (*)		
5D	*Glut4:* 0.0453 (*) *Insr*: 0.0007 (***) *Adcy4*: 0.0092 (**)		
5E	*Acc1*: 0.0353 (*) *Acc2*: 0.0213 (*) *Fas*: 0.0158 (*) *Scd2*: 0.0340 (*) *Hsl*: 0.0021 (**) *Atgl*: 0.0353 (*) *Pnpla3*: 0.0047 (**) *Apoc1*: 0.0062 (**)		
	Vehicle versus CL		
6A – *Gpr120*	0.0028 (**)		
6A – *Ucp1*	0.0016 (**)		

	Undiff versus Diff	**Undiff versus Diff + CL**	**Diff versus Diff + CL**
6B – *Gpr120*	n.d.	n.d.	BA: 0.0000 (***)
6B – *Ucp1*	n.d.	n.d.	BA: 0.0000 (***)
	WT vehicle versus WT TUG-891	**WT vehicle versus KO vehicle**	**WT vehicle versus KO TUG-891**
6C	Day 0: n.d. Day 7: 0.0015 (**)	Day 0: n.d. Day 3: 0.0050 (**) Day 7: 0.0001 (***) Day 9: 0.0001 (***)	Day 0: n.d. Day 3: 0.0052 (**) Day 7: 0.0001 (***) Day 9: 0.0001 (***)
6D – *aP2*	Day 0: n.d.	Day 0: n.d. Day 3: 0.099 (**) Day 7: 0.0001 (***) Day 9: 0.0001 (***)	Day 0: n.d. Day 3: 0.0017 (**) Day 7: 0.0001 (***) Day 9: 0.0001 (***)
6D – *Ucp1*	Day 0: n.d.	Day 0: n.d. Day 7: 0.0001 (***) Day 9: 0.0001 (***)	Day 0: n.d. Day 7: 0.0001 (***) Day 9: 0.0001 (***)
	TUG-891 versus vehicle	**TUG-891 versus TUG-891 + AH7614**	**TUG-891 + AH7614 versus vehicle**
7A	23 min: 0.0001 (***) 30 min: 0.0000 (***) 38 min: 0.0000 (***) 45 min: 0.0000 (***)	23 min: 0.0033 ($^{\#\#}$) 30 min: 0.0006 ($^{\#\#\#}$) 38 min: 0.0013 ($^{\#\#}$) 45 min: 0.0017 ($^{\#\#}$)	n.d.
	TUG-891 versus vehicle	**TUG-891 versus TUG-891 + BAPTA**	**TUG-891 + BAPTA versus vehicle**
7D	23 min: 0.0005 (***) 30 min: 0.0009 (***) 38 min: 0.0004 (***) 45 min: 0.0003 (***) 53 min: 0.0002 (***) 60 min: 0.0000 (***)	23 min: 0.0138 ($^{\#}$) 30 min: 0.0415 ($^{\#}$) 38 min: 0.0334 ($^{\#}$) 45 min: 0.0211 ($^{\#}$) 53 min: 0.0238 ($^{\#}$) 60 min: 0.0288 ($^{\#}$)	n.d.
	Basal versus 10 min		
7F	TUG-891: 0.0094 (**)		
	Vehicle versus TUG-891		
S3A	0.0483 (*)		
S3F	*Scd1*: 0.0001 (***)		
S3G	*Acc1:* 0.0455 (*) *Scd1:* 0.0267 (*) *Ccnb:* 0.0149 (*)		
SGH	*Dgat2:* 0.0441 (*) *Ccna:* 0.0003 (***) *Ccnb:* 0.0037 (**) *Mki67:* 0.0010 (***) *Ucp1:* 0.0157 (*)		
	Vehicle versus TUG-891		
S4C	0.0227 (*)		
	WT vehicle versus WT TUG-891	**WT vehicle versus KO vehicle**	**WT vehicle versus KO TUG-891**
S6A	Liver: 0.0000 (***) iBAT: 0.0023 (**)	n.s.	Liver: 0.0000 (***)
S6B	n.s.	n.s.	Liver: 0.0444 (*)
	Vehicle versus CL		
S8A	0.0362 (*)		

S8D	0.0005 (***)		
	WT TUG-891 versus UCP1 KO TUG-891		
S9A	10 µM: 0.0092 (**) 20 µM: 0.0144 (*) 30 µM: 0.0337 (*) 40 µM: 0.0211 (*) 60 µM: 0.0143 (*) 90 µM: 0.0003 (***) 100 µM: 0.0002 (***)		
	WT 1 mM GDP versus WT 3 mM GDP		
S9B	20 µM: 0.0359 (*)		
	40 µM: 0.0402 (*) 50 µM: 0.0074 (**) 60 µM: 0.0364 (*) 80 µM: 0.0121 (*) 90 µM: 0.0064 (**) 100 µM: 0.0112 (*) 110 µM: 0.0214 (*)		
	Vehicle versus TUG-891	**Vehicle versus forskolin**	**TUG-891 versus forskolin**
S9D	n.s.	0.0211 (*)	n.d.

N.s.: non-significant, n.d: non-determined. All P-values are rounded to 4 decimals.

Appendix Figure S1. TUG-891 non-significantly affects gene expression in skeletal muscle. Expression of markers for inflammation (*Cd68* and *Lgals3*) fibrosis (*Ctgf*), atrophy (*Gadd45a* and *Murf1*) and regeneration (*Myog*) were determined in skeletal muscle tissue of mice treated with vehicle or TUG-891 by qRT-PCR. Data represent means ± SEM (*n* = 8 per group).

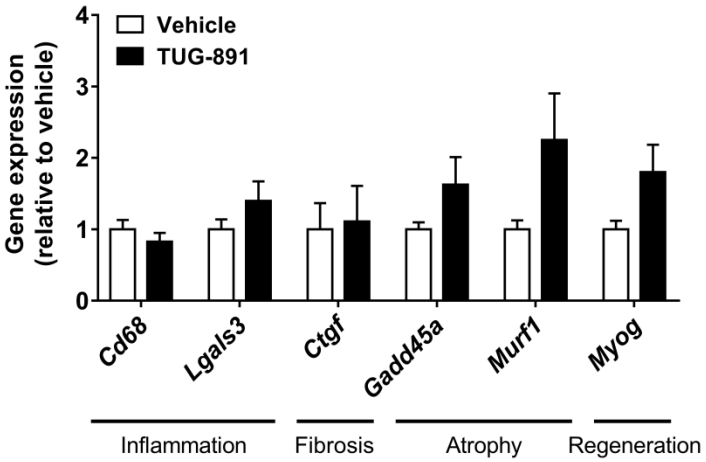

Appendix Figure S2. TUG-891 does not affect energy expenditure or physical activity levels. Energy expenditure (EE) (A) and physical activity (B) were determined by housing the mice individually in metabolic cages. Injection of TUG-891 or vehicle is indicated by dotted lines, and light and grey areas represent the light and dark phase, respectively. For bar graph analysis, mean results in the light and dark phase were calculated. Data represent means ± SEM (*n* = 8 per group).

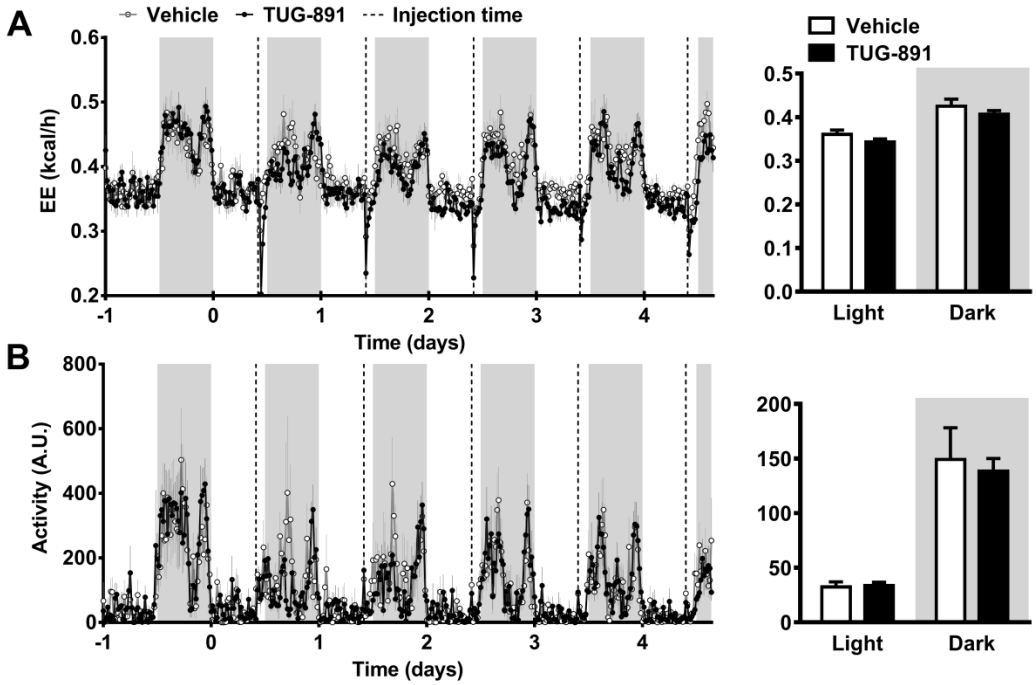

Appendix Figure S3. TUG-891 increases gene expression of markers for proliferation and thermogenesis in WAT. Plasma triglycerides (TG) (A), protein levels of UCP1, $pHSL_{563}$ and pPKA substrates in BAT (B-E), and gene expression markers for lipolysis, lipogenesis, proliferation and thermogenesis in BAT (F) and WAT (G-H) were determined in vehicle and TUG-891-treated mice. Data represent means ± SEM (n = 8 per group). * P < 0.05, ** P < 0.01, *** P < 0.001 compared to the vehicle group, according to the two-tailed unpaired Student's T test. The exact P-value for each significant difference can be found in Appendix Table S5.

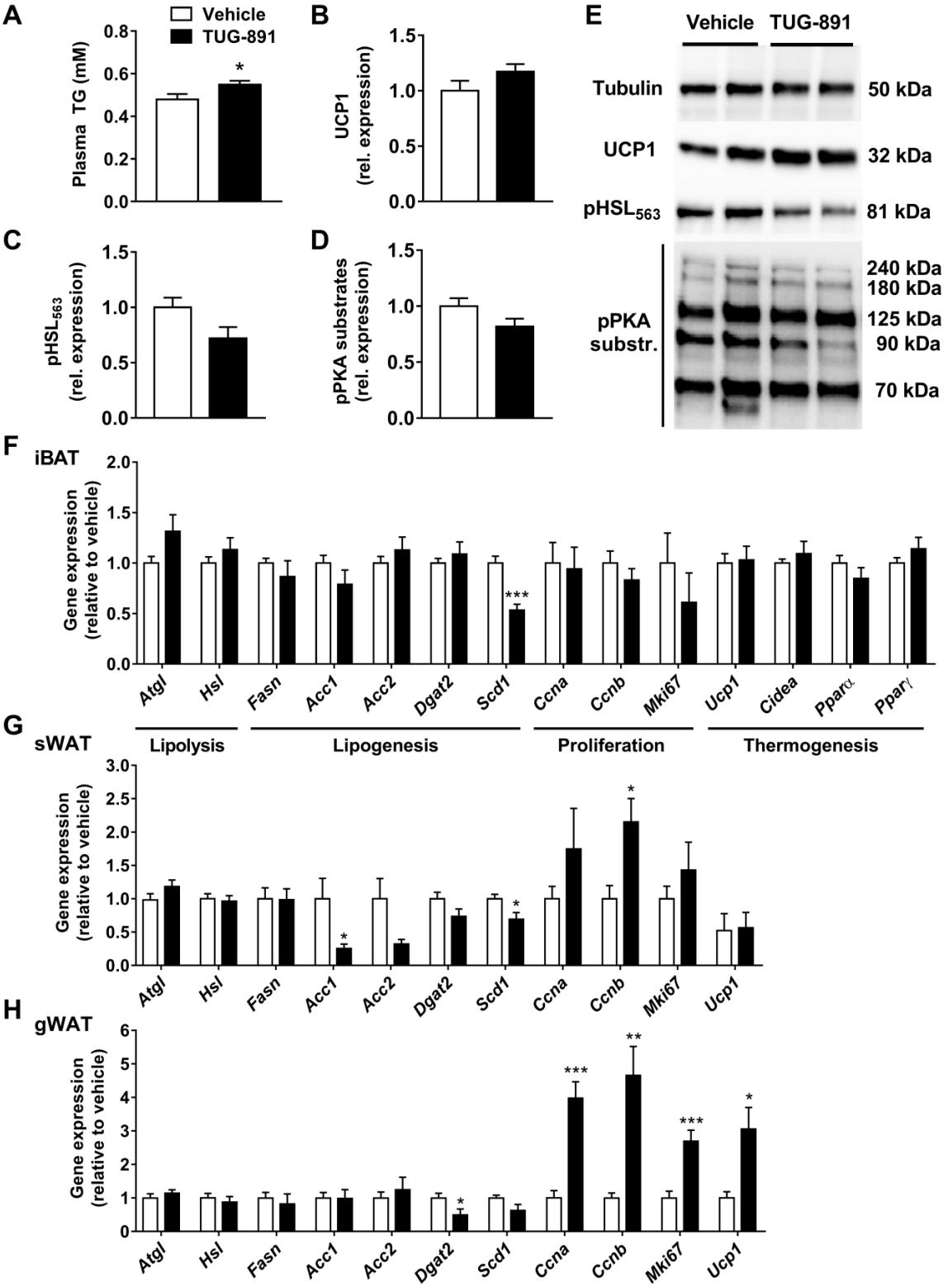

Appendix Figure S4. TUG-891 increases protein expression of UCP1 in gWAT. Representative images of UCP1 immunostained interscapular BAT (iBAT, A), subcutaneous WAT (sWAT, B) and gonadal WAT (gWAT, C) of mice treated with vehicle or the GPR120 agonist TUG-891. Stained slides were digitalized and relative UCP1 staining per area was analysed using ImageJ software. Data represent means ± SEM (n = 8 per group). * $P < 0.05$ compared to the vehicle group, according to the two-tailed unpaired Student's T test. The exact P-value for each significant difference can be found in Appendix Table S5.

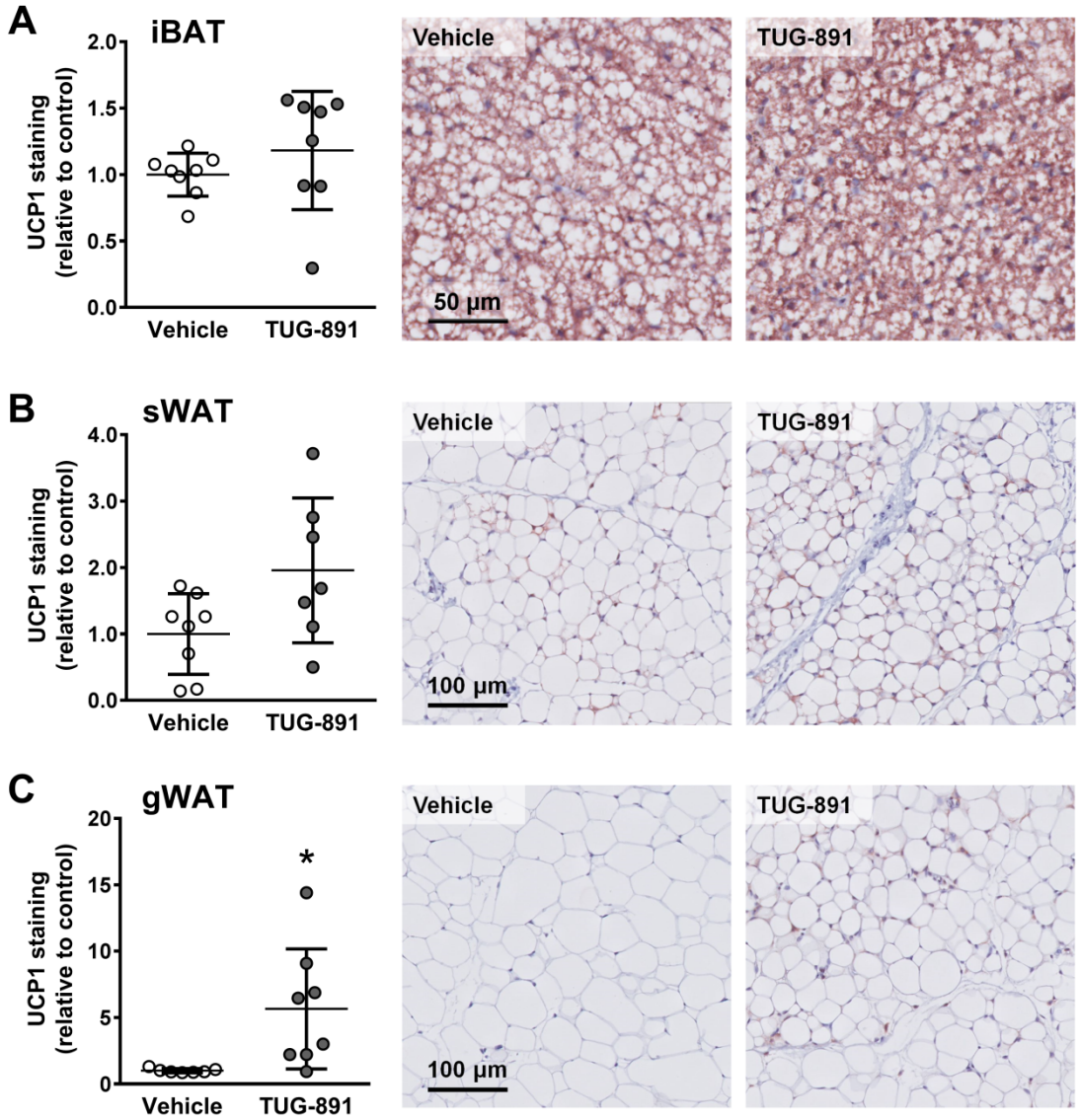

Appendix Figure S5. Respiratory exchange ratio and fat oxidation is similar between wild type and GPR120-deficient mice. Respiratory exchange ratio (RER) (A) and fat oxidation (B) was determined by housing GPR120 KO mice (n = 6) and WT littermates (n = 13) in metabolic cages. Light and grey areas represent the light and dark phase, respectively. For bar graph analysis, mean results in light and dark phase were calculated. Data represent means ± SEM.

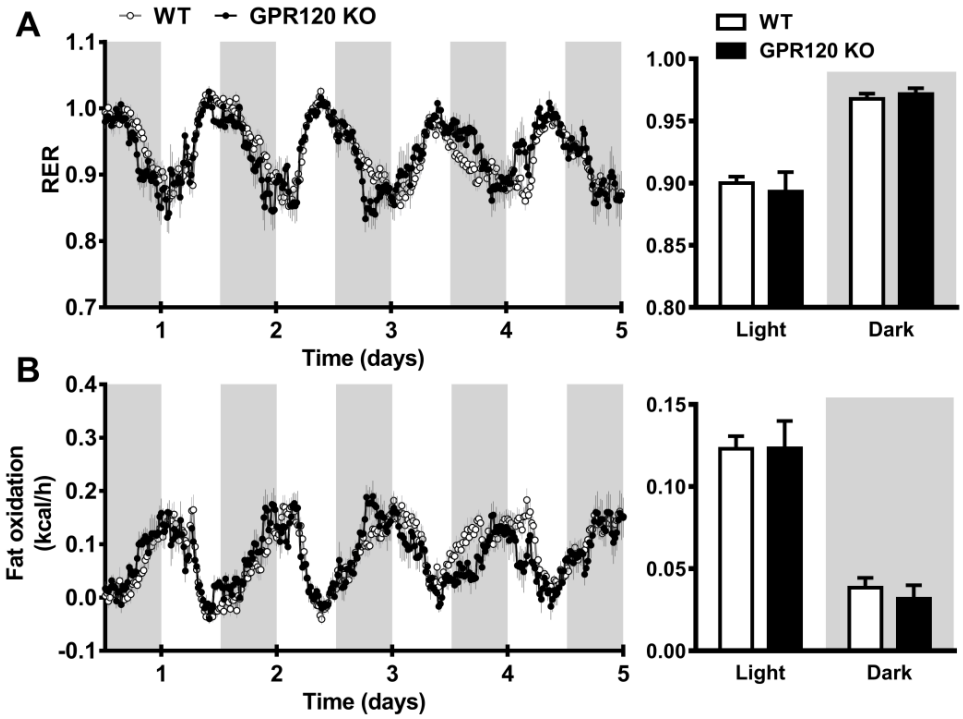

Appendix Figure S6. TUG-891 increases whole organ uptake of fatty acids by BAT. WT and GPR120 KO mice treated with vehicle or the GPR120 agonist TUG-891 were intravenously injected with glycerol tri[^{3}H]oleate ([^{3}H]TO)-labeled lipoprotein-like emulsion particles and [^{14}C]deoxyglucose ([^{14}C]DG). After 15 min, mice were sacrificed and uptake of [^{3}H]TO- and [^{14}C]DG-derived radioactivity (A-B) per whole organ was determined in organs that were dissected quantitatively, including gonadal WAT (gWAT) and interscapular BAT (iBAT). Data represent means ± SEM (n = 6-8 per group). * P < 0.05, ** P < 0.01, *** P < 0.001 compared to the vehicle group or indicated control group, according to two-way ANOVA with Tukey's post hoc test (A-B). The exact P-value for each significant difference can be found in Appendix Table S5.

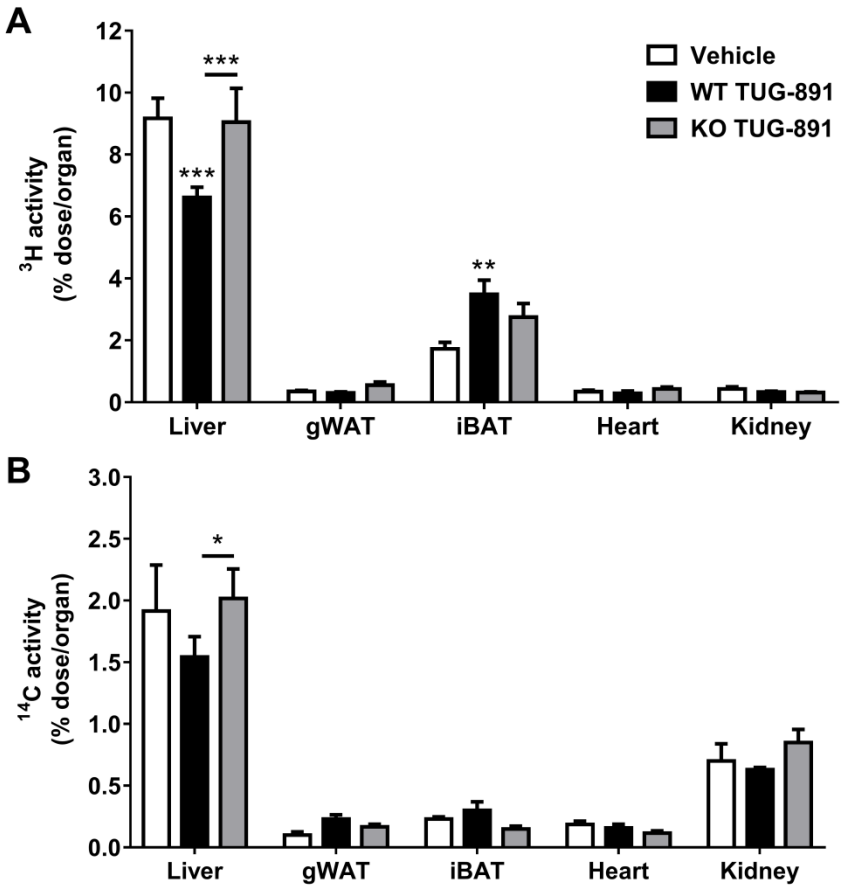

Appendix Figure S7. *Gpr120* is most highly expressed in BAT. *Gpr120* gene expression was determined in various tissues of FVB/N female mice, including brown adipose tissue (BAT), subcutaneous white adipose tissue (sWAT) and gonadal white adipose tissue (gWAT). Data represent means ± SEM (n = 3).

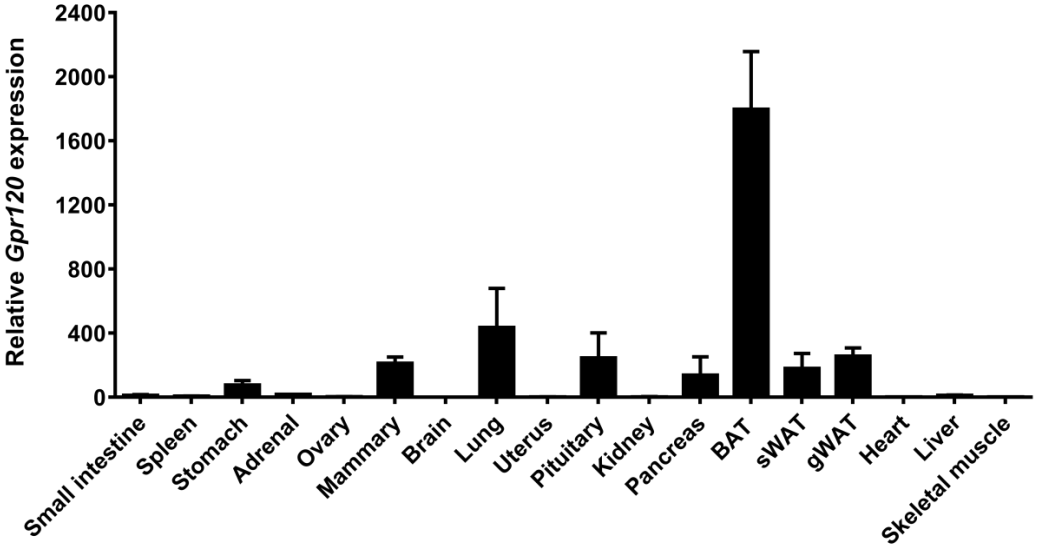

Appendix Figure S8. Gene expression profiles of *aP2*, *Cidea*, *Pref1* and *Adrb3* validate the immortalized murine brown adipocyte cell line. Immortalized murine brown adipocytes were differentiated for 0, 2, 4, 6, or 7 days after which expression of *aP2* (A), *Cidea* (B), *Pref1* (C), and *Adrb3* (D) was determined by qRT-PCR. On day 7, a subset of adipocytes was additionally stimulated with CL (10 μM). Data represent means ± SEM (n = 3). * P < 0.05, *** P < 0.001 compared to the vehicle group, according to the two-tailed unpaired Student's T test. The exact P-value for each significant difference can be found in Appendix Table S5.

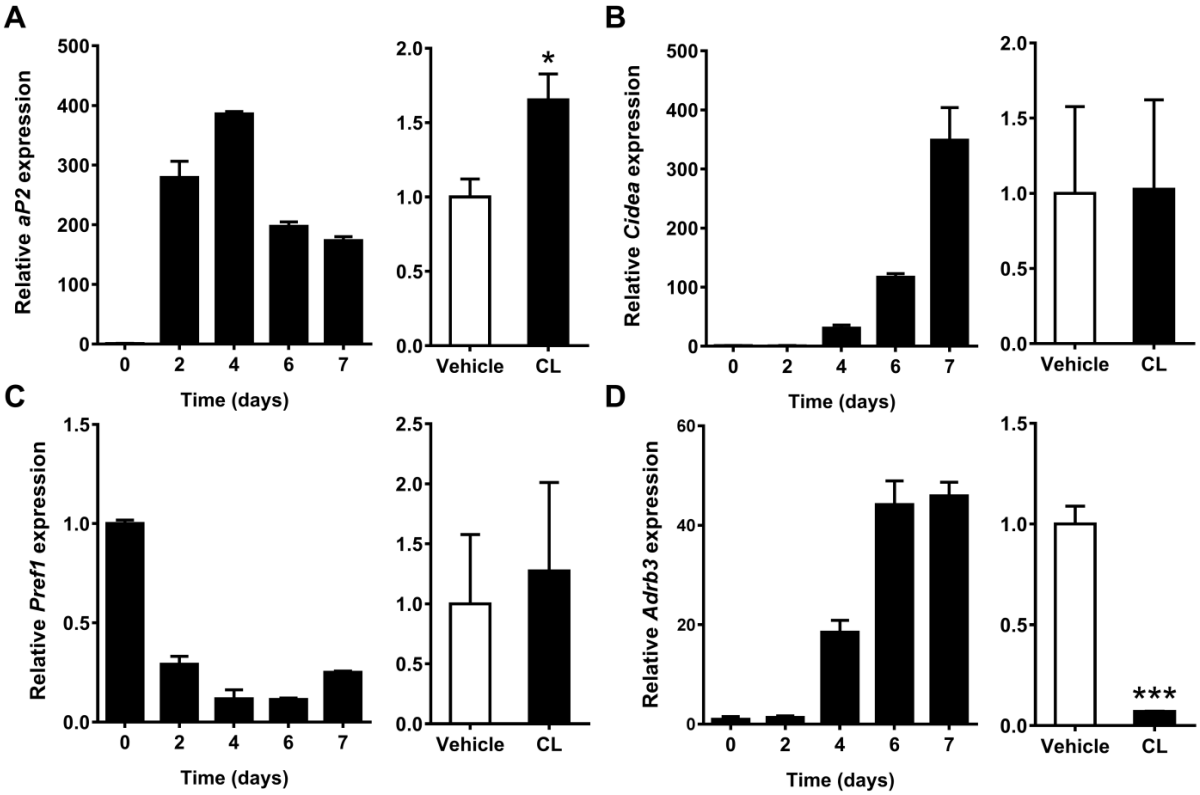

Appendix Figure S9. TUG-891 activates UCP1 by competitively interacting with GDP, but does not stimulate respiration through cAMP, ERK or AKT. Isolated mitochondria from WT and UCP1 KO mice (*n* = 4-5) were stimulated with TUG-891 or vehicle and mitochondrial oxygen consumption was measured (A, compilation of data shown in Figure 7B and C). TUG-891-induced mitochondrial respiration was measured in the presence of 1 or 3 μM GDP, in WT (B) and UCP1 KO (C) mitochondria (*n* = 3-5). Intracellular cAMP levels were measured in differentiated brown adipocytes pretreated with vehicle, TUG-891 (10 μM) or forskolin (10 μM) (*n* = 7) for 5 min. (D). Primary brown adipocytes (*n* = 2) were stimulated for 5 min with vehicle or TUG-891 (10 μM) and relative amounts of phosphorylated and total protein was determined by Western blotting. The amount of phosphorylated protein was normalized to the total amount of protein (E). Immortalized brown adipocytes (*n* = 5-6) were pretreated for 30 min with vehicle, U0126 (10 μM) or AKT1/2 kinase inhibitor (10 μM), after which the OCR was determined in a Seahorse XF24 analyzer. After three baseline measurements, either vehicle or TUG-891 (10 μM) was injected into the wells (F & G). Brown adipocytes were incubated with the calcium sensitive dye Fluo-4-AM for 1 h at RT, followed by live cell imaging with a spinning disk confocal (UltraVIEW Vox, PerkinElmer) and stimulation with TUG-891 (10 μM) with or without the presence of YM-254890 (0.1 μM) (H). F_1/F_0 represents peak fluorescence divided by baseline fluorescence. Data represent means ± SEM. * $P < 0.05$, * $P < 0.01$, *** $P < 0.001$ compared to the control group, according to the two-tailed unpaired Student's T test (A-B) or one-way ANOVA with Dunnett's post hoc test (C). The exact *P*-value for each significant difference can be found in Appendix Table S5.

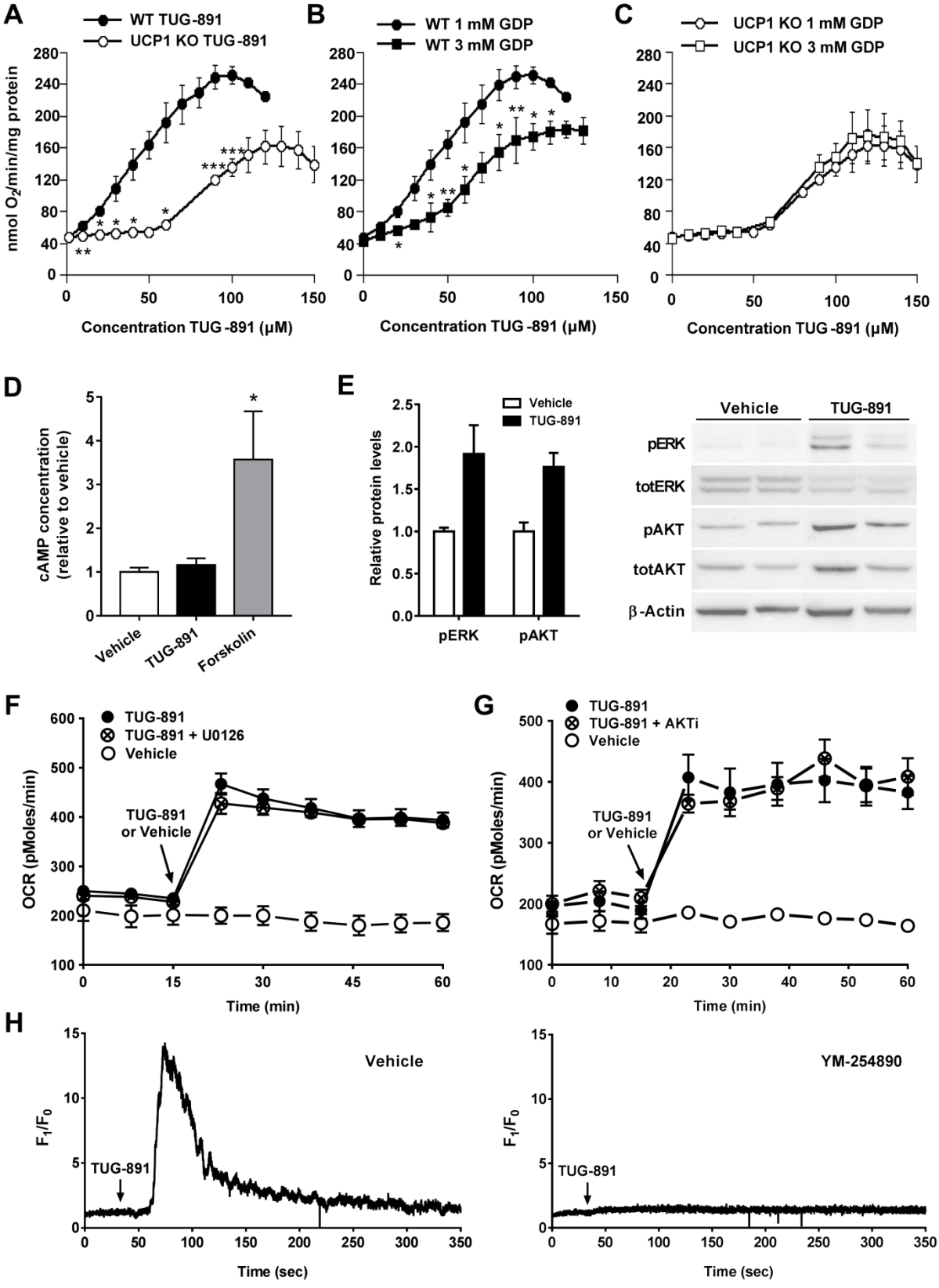
A
WT TUG-891
UCP1 KO TUG-891
nmol O2/min/mg protein
Concentration TUG-891 (μM)
B
WT 1 mM GDP
WT 3 mM GDP
Concentration TUG-891 (μM)
C
UCP1 KO 1 mM GDP
UCP1 KO 3 mM GDP
Concentration TUG-891 (μM)
D
cAMP concentration (relative to vehicle)
Vehicle
TUG-891
Forskolin
E
Vehicle
TUG-891
Relative protein levels
pERK
pAKT
Vehicle
TUG-891
pERK
totERK
pAKT
totAKT
β-Actin
F
TUG-891
TUG-891 + U0126
Vehicle
TUG-891 or Vehicle
OCR (pMoles/min)
Time (min)
G
TUG-891
TUG-891 + AKTi
Vehicle
TUG-891 or Vehicle
OCR (pMoles/min)
Time (min)
H
Vehicle
TUG-891
F1/F0
Time (sec)
YM-254890
TUG-891
F1/F0
Time (sec)